The NH_4^+-NO_3^--Cl^--SO_4^{2-}-H_2O aerosol system and its gas phase precursors at a pasture site in the Amazon Basin: How relevant are mineral cations and soluble organic acids?

Ivonne Trebs,[1] Swen Metzger,[1] Franz X. Meixner,[1] Günter Helas,[1] András Hoffer,[1] Yinon Rudich,[2] Alla H. Falkovich,[2] Marcos A. L. Moura,[3] Rosiberto S. da Silva Jr.,[3] Paulo Artaxo,[4] Jacob Slanina,[5] and Meinrat O. Andreae[1]

Received 30 September 2004; revised 4 January 2005; accepted 9 February 2005; published 6 April 2005.

[1] Real-time measurements of ammonia, nitric acid, hydrochloric acid, sulfur dioxide and the water-soluble inorganic aerosol species, ammonium, nitrate, chloride, and sulfate were performed at a pasture site in the Amazon Basin (Rondônia, Brazil). The measurements were made during the late dry season (biomass burning), the transition period, and the onset of the wet season (clean conditions) using a wet-annular denuder (WAD) in combination with a Steam-Jet Aerosol Collector (SJAC). Measurements were conducted from 12 September to 14 November 2002 within the framework of LBA-SMOCC (Large-Scale Biosphere Atmosphere Experiment in Amazonia - Smoke Aerosols, Clouds, Rainfall, and Climate: Aerosols From Biomass Burning Perturb Global and Regional Climate). Real-time data were combined with measurements of sodium, potassium, calcium, magnesium, and low-molecular weight (LMW) polar organic acids determined on 12-, 24-, and 48-hours integrated filter samples. The contribution of inorganic species to the fine particulate mass ($D_p \leq 2.5$ μm) was frequently below 20% by mass, indicating the preponderance of organic matter. The measured concentration products of $NH_3 \times HNO_3$ and $NH_3 \times HCl$ persistently remained below the theoretical equilibrium dissociation constants of the $NH_3/HNO_3/NH_4NO_3$ and $NH_3/HCl/NH_4Cl$ systems during daytime (RH < 90%). The application of four thermodynamic equilibrium models (EQMs) indicates that the fine mode aerosol anions NO_3^-, Cl^-, and SO_4^{2-} were balanced predominantly by mineral cations (particularly pyrogenic K^+) during daytime. At nighttime (RH > 90%) fine-mode NH_4NO_3 and NH_4Cl are predicted to be formed in the aqueous aerosol phase. Probably, Cl^- was driven out of the aerosol phase largely by reaction of pyrogenic KCl with HNO_3 and H_2SO_4. As shown by an updated version of the equilibrium simplified aerosol model (EQSAM2), which incorporates mineral aerosol species and lumped LMW polar organic acids, daytime aerosol NH_4^+ was mainly balanced by organic compounds.

Citation: Trebs, I., et al. (2005), The NH_4^+-NO_3^--Cl^--SO_4^{2-}-H_2O aerosol system and its gas phase precursors at a pasture site in the Amazon Basin: How relevant are mineral cations and soluble organic acids?, *J. Geophys. Res.*, *110*, D07303, doi:10.1029/2004JD005478.

1. Introduction

[2] Widespread biomass burning emissions in the Amazon Basin significantly alter the chemical properties of the tropical pristine background atmosphere. This is reflected by elevated levels of carbon monoxide (CO), carbon dioxide (CO_2), nitric oxides (NO_x), ozone (O_3) and hydrocarbons (in particular methane (CH_4)) [*Crutzen and Andreae*, 1990]. When biomass burning takes place, particle number concentrations are enhanced by an order of magnitude compared to the clean conditions present during the wet season [*Andreae et al.*, 2002; *Artaxo et al.*, 2002; *Guyon et al.*, 2003]. Amazonian aerosol particles consist to a large extent of organic matter, which often accounts for 90% of the total aerosol mass, and 45% to 75% of the organic carbon (OC) is water-soluble [*Andreae and Crutzen*, 1997; *Mayol-Bracero et al.*, 2002; *Graham et al.*, 2003a]. Although inorganic aerosol compounds, mainly comprising ammonium (NH_4^+), nitrate (NO_3^-), chloride

[1]Biogeochemistry and Air Chemistry Departments, Max Planck Institute for Chemistry, Mainz, Germany.
[2]Department of Environmental Sciences, Weizmann Institute, Rehovot, Israel.
[3]CCEN-Departamento de Meteorologia, Universidad Federal de Alagoas, Alagoas, Brazil.
[4]Instituto de Física, Universidade de São Paulo, São Paulo, Brazil.
[5]Department of Environmental Sciences, University of Wageningen, Wageningen, Netherlands.

0148-0227/05/2004JD005478

(Cl^-), potassium (K^+), and sulfate (SO_4^{2-}), are minor components of Amazonian aerosols, they play a major role in the nucleation and growth of cloud droplets [*Roberts et al.*, 2002]. Additionally, they may contribute efficiently to direct aerosol radiative forcing, which is strongly influenced by the water uptake of aerosols that accompanies an increase in RH [*Pilinis et al.*, 1995]. In turn, aerosol chemical composition determines the water uptake as a function of ambient RH, and, concomitantly a change in RH affects gas/aerosol partitioning processes, hence increasing or decreasing the amount of semivolatile aerosol species [*Metzger*, 2000].

[3] Primary inorganic aerosol constituents such as sea-salt (NaCl) and mineral cations (K^+, Ca^{2+}, Mg^{2+}) originate from sea-spray emissions and from soil dust or biomass burning emissions, respectively. These aerosol species are predominantly present in coarse mode aerosols ($D_p > 2.5$ μm). The fine mode of pyrogenic (biomass-burning derived) aerosols ($D_p \leq 2.5$ μm) usually contains a sizeable amount of K^+ [*Andreae*, 1983]. All other inorganic aerosol components (NH_4^+, NO_3^-, SO_4^{2-} and to some extent Cl^-) are formed by gas-to-particle conversion processes. Among these so-called secondary aerosol species, NH_4^+ and SO_4^{2-} are mostly found in fine mode aerosols, whereas aerosol NO_3^- and Cl^- usually have bimodal size distributions. The presence of primary inorganic aerosol species sets up the initial aerosol inorganic composition by forming nonvolatile salts (e.g., KCl, $NaNO_3$, and $CaSO_4$). Semivolatile compounds, such as ammonium nitrate (NH_4NO_3) and ammonium chloride (NH_4Cl) are thought to form via reversible phase equilibria with gaseous ammonia (NH_3), nitric acid (HNO_3) and hydrochloric acid (HCl) [*Pio and Harrison*, 1987; *Stelson et al.*, 1979]. These gas/aerosol equilibria are strongly dependent on ambient RH, temperature (T) and aerosol chemical composition. In chemical systems composed of NH_3, HNO_3, HCl, and H_2SO_4, the formation of nonvolatile $(NH_4)_2SO_4$ is preferred [*Seinfeld and Pandis*, 1998]. Only when NH_3 is available in excess of H_2SO_4 and when favorable meteorological conditions (low to moderate T and/or high RH) prevail, neutralization of HNO_3 and HCl vapor occurs. NH_3 and HCl are directly emitted by biomass fires [*Hegg et al.*, 1988; *Andreae et al.*, 1996], whereas the primary source of HNO_3 is the reaction of NO_2 with the OH radical in the troposphere during daytime. HNO_3, HCl, H_2SO_4 and their salts are highly hygroscopic, therefore, aerosol-associated water plays a key role in gas/aerosol partitioning processes, particularly under very humid conditions in the tropics. An increase in RH causes the water activity of the aerosols to increase, leading to a decrease of solute molality which results in condensation of NH_3, HNO_3 and HCl vapor [*Metzger et al.*, 2002].

[4] Commonly, the simulation of gas/aerosol partitioning processes for inorganic compounds is performed by applying so-called thermodynamic equilibrium models (EQMs). Generally, EQMs are suitable to predict inorganic aerosol behavior for the NH_4^+-NO_3^--Cl^--SO_4^{2-}-H_2O system as shown by box model studies in temperate regions [e.g., *Ansari and Pandis*, 2000; *Ueda et al.*, 2000; *Zhang et al.*, 2003; *Kuhns et al.*, 2003]. As reported by *Fridlind and Jacobson* [2000] an EQM approach for inorganic species could explain observations over the Southern Ocean, where equilibrium was achieved between HNO_3 and fine mode aerosol NO_3^-. However, during that study, organic matter was not a dominant component of the measured aerosol. A possible effect of the presence of organic compounds on the inorganic gas/aerosol equilibrium was indicated by *Zhang et al.* [2003]. Although some attempts have been made to calculate the thermodynamic properties of soluble mixed inorganic/organic aerosols [e.g., *Clegg et al.*, 2001; *Pankow*, 2003], most of the widely used EQMs include inorganic aerosol species only.

[5] To date, no information is available about inorganic gas/aerosol partitioning processes in the tropics. The first real-time measurements of NH_3, HNO_3, HCl, SO_2 and their chemically related aerosol species NH_4^+, NO_3^-, Cl^- and SO_4^{2-} have been performed by us at a pasture site in southwest Amazonia (Rondônia, Brazil) [*Trebs et al.*, 2004] during the LBA-SMOCC 2002 campaign (Large Scale Biosphere Atmosphere Experiment in Amazonia, Smoke Aerosols, Clouds, Rainfall and Climate: Aerosols from Biomass Burning Perturb Global and Regional Climate) [*Andreae et al.*, 2004]. In the present work we will use these results to study the characteristics of the inorganic gas/aerosol system in the Amazon Basin, which are expected to be mainly controlled by (1) high RH and high temperatures, (2) the presence of mineral cations in the fine and coarse aerosol fraction, and (3) the dominance of organic matter. Diel variations of measured inorganic compounds in gas and aerosol phase and gas/aerosol partitioning coefficients (ratios aerosol/(gas + aerosol)) for ammonium, nitrate and chloride will be discussed in detail. The fine mode aerosol ion balance in this region is studied by considering also mineral cations (K^+, Ca^{2+} and Mg^{2+}) and low molecular weight (LMW) organic acids obtained from the analysis of aerosols collected on 12-, 24- and 48-hours integrated filter samples. Additionally, an evaluation of the thermodynamic equilibrium assumption under ambient conditions present at the measurement site is performed. We have applied four different EQMs, namely SCAPE2 [*Kim et al.*, 1993; *Kim and Seinfeld*, 1995; *Meng et al.*, 1995], ISORROPIA [*Nenes et al.*, 1998], GEFMN [*Ansari and Pandis*, 1999b], and EQSAM [*Metzger et al.*, 2002] to gain detailed insights into formation pathways of inorganic aerosol constituents under tropical conditions and to assess the influence of mineral cations on gas/aerosol partitioning processes. Information about the possible effect of LMW organic acids on the inorganic gas/aerosol system will be deduced from simulations using an updated version of EQSAM (henceforth referred to as EQSAM2), which includes lumped organic acids in addition to sea-salt and mineral cations (S. Metzger and J. Lelieveld, manuscript in preparation, 2005).

2. Site Description and Methods

2.1. Measurement Site

[6] Field measurements were performed at a pasture site in the state of Rondônia, Brazil (Fazenda Nossa Senhora Aparecida (FNS), 10°45′44″S, 62°21′27″W, 315 m asl) located in the south-western part of the Amazon Basin. During the last 25 years, Rondônia has been progressively cleared of rain forest by slash and burn activities. The vegetation at FNS is dominated by grass (*Brachiaria brizantha*) with small patches of *Brachiaria humidicola*

and very few isolated palms and bushes. The pasture is used as a cattle ranch. Near the site, flat hills (300 to 440 m) are located at a distance of 3 to 4 km. The towns Ouro Preto do Oeste (~40,800 inhabitants) and Ji-Paraná (~110,000 inhabitants) are situated approximately 8 km and 40 km to the ENE and ESE of the site, respectively. FNS is affected by widespread vegetation fires occurring every year in the state of Rondônia during the dry season (June through September). A more detailed description of the measurement site is given in *Andreae et al.* [2002] and *Kirkman et al.* [2002].

2.2. WAD/SJAC Sampling and Analysis

[7] Air was sampled at a height of 530 cm above ground through a vertical polyethylene conduit with an inner diameter of 7 cm, protruding 150 cm above and 50 cm away from an air-conditioned wooden house where the sampling and analytical equipment was located. A subsample of the air was aspirated from the center of the conduit's cross section area through a steel elbow (90° angle of steel tubing, inner surface PFA Teflon coated) or alternatively through a pre-impactor (PM 2.5 size cut; type 413, University Research Glassware, aluminum cyclone, PFA Teflon coated). Aerosol samples of either PM 2.5 ($D_p \leq 2.5$ μm) or total suspended particulate matter (TSP) were collected in alternating cycles (1–3 days). Soluble gases (NH_3, HNO_3, HCl and SO_2) were collected by a horizontally aligned, rotating wet-annular denuder (WAD) [*Wyers et al.*, 1993] which was continuously coated with a 10^{-4} M carbonate solution. Inorganic aerosol species (NH_4^+, NO_3^-, Cl^- and SO_4^{2-}) were sampled continuously with a Steam-Jet Aerosol Collector (SJAC) [*Khlystov et al.*, 1995]. The resulting aqueous solutions of aerosol and gas were analyzed on-line using ion chromatography (IC) for anions and flow injection analysis (FIA) for ammonium (NH_4^+). Measurement intervals were set to 20 min (biomass burning season), 40 min (transition period) and 60 min (wet season). The measurement uncertainties of ambient mixing ratios as determined by Gaussian error propagation were below 15% [cf. *Trebs et al.*, 2004]. The median limit of detection (LOD = 3σ) was below 0.015 ppb for HNO_3/NO_3^-, HCl/Cl^- and SO_2/SO_4^{2-} and was below 0.118 ppb for NH_3/NH_4^+ [cf. *Trebs et al.*, 2004]. A detailed description and verification of the measurement method and of the inlet system can be found in *Slanina et al.* [2001] and *Trebs et al.* [2004].

2.3. Supporting Measurements

[8] In addition to the WAD/SJAC measurements, the following meteorological quantities were measured by an automatic weather station (AWS, 1 minute time resolution): wind speed and direction, air temperature, relative humidity, global radiation and surface wetness. The AWS was situated at a distance of ~20 m from the inlet of the WAD/SJAC system.

[9] The total particulate mass (PM 2.5 and PM 10) was measured on-line with an ambient particulate monitor (TEOM Series 1400a, Rupprecht & Patashnick Co., Inc). Furthermore, the overall inorganic and organic aerosol composition was determined using traditional filter sampling methods. Depending on the atmospheric aerosol concentration, the filter sampling periods were 12 hours daytime, 12 hours nighttime, 24 hours, and 48 hours. During the 24 and 48 hours sampling periods, sampling was performed during 2 or 3 consecutive days or nights, respectively. Aerosol samples (PM 2.0 and PM 10) were collected on Nuclepore filters using a Stacked Filter Unit (SFU) [*Falkovich et al.*, 2005]. The filter sampler was mounted at a height of 4 m above ground. Samples were stored at −25°C until analysis. Standard cation analyses were performed using a HPLC system (Varian ProStar; Detector: Dionex ED50 electrochemical detector) [cf. *Falkovich et al.*, 2005].

[10] Fine mode aerosols (PM 2.5, $D_p \leq 2.5$ μm) were collected simultaneously on quartz filters (Pallflex Tissuquartz 2500 QAT-UP) using a high-volume dichotomous sampler (HVDS) [see *Mayol-Bracero et al.*, 2002, and references therein]. The sampling system was mounted on a tower 10 m above ground level. Loaded filters were placed in a prebaked glass jar and stored at −25°C until analysis. HVDS samples were analyzed by gas chromatography-mass spectrometry (GC/MS) for LMW polar organic acids [cf. *Graham et al.*, 2003b].

2.4. Thermodynamic Equilibrium Models (EQMs)

[11] Four different EQMs, SCAPE2 [*Kim and Seinfeld*, 1995; *Kim et al.*, 1993; *Meng et al.*, 1995], ISORROPIA [*Nenes et al.*, 1998], GEFMN [*Ansari and Pandis*, 1999b], and EQSAM2 [*Metzger et al.*, 2002; S. Metzger and J. Lelieveld, manuscript in preparation, 2005] were applied to simulate gas/aerosol partitioning at FNS. Table 1 shows the major features of these EQMs. All EQMs are based on the assumption that aerosol particles are internally mixed and that thermodynamic equilibrium exists between gas and aerosol phase. Based on these assumptions, EQMs explicitly calculate the equilibrium composition of the liquid or solid aerosol phase. The existence of an aqueous phase is determined by the lowest deliquescence RH of an inorganic salt compound (e.g., NH_4NO_3), or a hygroscopic salt mixture. It is generally agreed that ambient RH is not influenced by the deliquescence of aerosol particles, because of the large amount of water vapor present in the atmosphere compared to the aerosol water mass [*Metzger*, 2000]. This implies, neglecting the Kelvin effect, that the aerosol water activity is equal to ambient RH [*Bassett and Seinfeld*, 1983].

[12] SCAPE2 is the most comprehensive EQM in terms of aerosol species considered, since it is the only model which explicitly incorporates mineral cations such as K^+, Ca^{2+} and Mg^{2+}, while ISORROPIA is the most sophisticated EQM in terms of numerical accuracy. In ISORROPIA and SCAPE2 the equilibrium constant is derived for each single reaction [*Ansari and Pandis*, 1999a]. This results in a complex system of nonlinear algebraic equations whose solution corresponds to a minimum of the Gibbs free energy. In contrast, the GEFMN model is based on an algorithm that directly minimizes the Gibbs free energy to meet the equilibrium condition of the system. Finally, the approach applied in EQSAM2 is the simplest one, since it uses a simplified, although rigorous, calculation of activity coefficients and solution molalities [*Metzger et al.*, 2002]. The EQSAM2 approach implies that for atmospheric aerosols in equilibrium with ambient air, an increase in, e.g., NH_4NO_3 as a result of decreasing temperature and increasing RH is always associated with the condensation of a

Table 1. Main Characteristics of the Thermodynamic Equilibrium Models Applied for the Simulation of Inorganic Gas/Aerosol Partitioning at FNS During LBA-SMOCC 2002[a]

		EQSAM2[b]	GEFMN[c]	ISORROPIA[d]	SCAPE2[e]
Species treated	Gas phase	NH_3, HNO_3, HCl, H_2O			
	Solid phase	Na_2SO_4 $NaHSO_4$ NaCl NH_4Cl NH_4NO_3 $(NH_4)_2SO_4$ NH_4HSO_4 $(NH_4)_3H(SO_4)_2$ KCl, K_2SO_4 $KHSO_4$,KNO_3 $CaCl_2$,$CaSO_4$ $Ca(NO_3)_2$, $MgCl_2$ $MgSO_4$, $Mg(NO_3)_2$	Na_2SO_4 $NaHSO_4$ NaCl NH_4Cl NH_4NO_3 $(NH_4)_2SO_4$ NH_4HSO_4 $(NH_4)_3H(SO_4)_2$	Na_2SO_4 $NaHSO_4$ NaCl NH_4Cl NH_4NO_3 $(NH_4)_2SO_4$ NH_4HSO_4 $(NH_4)_3H(SO_4)_2$	Na_2SO_4 $NaHSO_4$ NaCl NH_4Cl NH_4NO_3 $(NH_4)_2SO_4$ NH_4HSO_4 $(NH_4)_3H(SO_4)_2$ KCl, K_2SO_4 $KHSO_4$,KNO_3 $CaCl_2$,$CaSO_4$ $Ca(NO_3)_2$, $MgCl_2$ $MgSO_4$, $Mg(NO_3)_2$
	Liquid phase	H^+, NH_4^+, Na^+, NO_3^-, Cl^-, SO_4^{2-}, HSO_4^-, H_2SO_4, H_2O OH^-, NH_3, Ca^{2+}, Mg^{2+}, K^+, LMW organic acids	H^+, NH_4^+, Na^+, NO_3^-, Cl^-, SO_4^{2-}, HSO_4^-, H_2SO_4, H_2O	H^+, NH_4^+, Na^+, NO_3^-, Cl^-, SO_4^{2-}, HSO_4^-, H_2SO_4, H_2O, OH^-, NH_3	H^+, NH_4^+, Na^+, NO_3^-, Cl^-, SO_4^{2-}, HSO_4^-, H_2SO_4, H_2O, OH^-, NH_3, Ca^{2+}, Mg^{2+}, K^+
Multicomponent activity coefficient method		Theoretically derived [*Metzger*, 2000]	[*Clegg et al.*, 1997]	Bromley Pitzer	Kusik-Meissner Bromley Pitzer
Binary activity method		Theoretically derived [*Metzger*, 2000]	N/A	Kusik-Meissner	Kusik-Meissner
Temperature dependence of DRH		YES	YES	YES	YES
Composition dependence of DRH		YES	YES	YES	NO
Divided composition domain		YES	NO	YES	YES
Water activity		ZSR (Zdanovskii, Stokes and Robinson-relation)			

[a]Parts of the table are taken from *Ansari and Pandis* [1999a].
[b]EQSAM2 uses a simplified approach to calculate the equilibrium composition by which not all chemical reactions are explicitly solved for the liquid/solid partitioning and the aerosol water content (instead they are partly based on cation and anion ratios). However, the solute molalities and the aerosol activity (including activity coefficients) are theoretically derived and thus not empirically or semiempirically in contrast to other approaches.
[c]GEFMN directly minimizes the Gibbs-free-energy based on thermodynamic data that are, however, not valid above RH > 94%.
[d]ISORROPIA calculates the equilibrium composition based on high numerical accuracy and on either of the (semiempirical) activity coefficient calculation methods depending on the aerosol composition.
[e]SCAPE2 explicitly treats mineral cations and has an option to choose between the semiempirical activity coefficient calculation methods. For this study, the Kusik-Meissner method was chosen.

certain amount of water vapor [*Metzger*, 2000]. Considering the change of aerosol water that is associated with an equilibrium reaction, the relationship between aerosol activity/solution molality and RH can be expressed using theoretically derived equations [*Metzger et al.*, 2002]. In this study we have applied an updated version of EQSAM (namely EQSAM2) that incorporates, besides sea-salt and mineral cations, lumped low molecular weight (LMW) polar organic acids, which, depending on their protonation constant, balance excess cations. The structure of EQSAM2 is the same as described in *Metzger* [2000], *Metzger et al.* [2002], and S. Metzger and J. Lelieveld (manuscript in preparation, 2005).

3. Results

[13] Field measurements during SMOCC comprised three sampling periods. The first was a period of extensive biomass burning activity during the late dry season (12–30 September), the second an intermediate phase (transition period, 01–31 October) and the third represented fairly clean conditions during the onset of the wet season (01–14 November). Due to an instrument failure, no samples were collected with the WAD/SJAC system from 24 September to 7 October. In this study, we focus mainly on a period during the dry season (biomass burning, 12–23 September). Meteorological data were averaged and synchronized according to the time series obtained with the WAD/SJAC system.

3.1. Gas and Aerosol Phase Mixing Ratios

[14] Tables 2a–2c present an overview of average mixing ratios for the dry season, transition period and wet season for all measured species considered in this study. Individually identifiable LMW polar organic acids determined in aerosol particles (collected with the SFU or HVDS sampler (PM 2.5)) are grouped into three chemical classes: (1) aliphatic mono-/di-/tricarboxylic acids (formic acid, acetic acid, oxalic acid, malonic acid, succinic acid, maleic acid, tricarballylic acid), (2) aliphatic oxo-/hydroxyacids (glyoxylic acid, glycolic acid, lactic acid, glyceric acid, hydroxymalonic acid, malic acid, citric acid), and (3) aromatic carboxylic acids (3-hydroxy-benzoic acid, 4-hydroxy-benzoic acid, vanillic acid, syringic acid, phthalic acid) [cf. *Falkovich et al.*, 2005]. The least and the most abundant species in each class determine the ranges given in Table 2c.

Table 2a. Average Mixing Ratios Plus or Minus Standard Deviation for NH_3, Aerosol NH_4^+, HNO_3, Aerosol NO_3^-, HCl, Aerosol Cl^-, SO_2, and Aerosol SO_4^{2-} (Measured With the WAD/SJAC System) During the Late Dry (Biomass Burning) Season (12–13 September), the Transition Period (7–31 October), and the Onset of the Wet Season (1–14 November) at FNS During LBA-SMOCC 2002

	NH_3, ppb	NH_4^+,[a] ppb	HNO_3, ppb	NO_3^-,[a] ppb	HCl, ppb	Cl^-,[a] ppb	SO_2, ppb	SO_4^{2-},[a] ppb
Dry season	2.22 ± 1.57	1.17 ± 0.69	0.19 ± 0.13	0.41 ± 0.30	0.17 ± 0.16	0.07 ± 0.06	0.15 ± 0.13	0.29 ± 0.11
Transition period	1.34 ± 1.19	0.61 ± 0.35	0.09 ± 0.07	0.12 ± 0.08	0.09 ± 0.08	0.03 ± 0.02	0.04 ± 0.03	0.14 ± 0.07
Wet season	0.72 ± 0.56	0.46 ± 0.19	0.07 ± 0.04	0.06 ± 0.02	0.05 ± 0.04	0.04 ± 0.05	0.08 ± 0.03	0.11 ± 0.04

[a]Data of TSP and PM 2.5 aerosol measurements were included in average values.

[15] Except for Na^+, mixing ratios of all compounds showed at least a 2-fold decrease from the dry season (biomass burning) to the wet season (clean conditions), indicating that biomass burning is a significant source of these species. Inorganic ionic aerosol composition at FNS was dominated by NH_4^+, being present in mixing ratios at least 3 times higher than other ions [*Trebs et al.*, 2004]. This was obviously caused by its gaseous precursor NH_3, which was an order of magnitude more abundant than other water-soluble trace gases (see Table 2a). Other important inorganic ions contributing to the fine aerosol mass (PM 2.5) at FNS were K^+, NO_3^- and SO_4^{2-}. Total PM 2.5 decreased on average from $\sim$ 100 $\mu g\ m^{-3}$ during the dry season, to 20 $\mu g\ m^{-3}$ during the transition period to about 5 $\mu g\ m^{-3}$ during the wet season (Figure 1, top). The contribution of inorganic species to PM 2.5 showed a 4-fold increase from dry season to wet season. However, the contribution of inorganic species to total PM 2.5 always remained below 20% (Figure 1, bottom). Neglecting a few other elements (e.g. Al, Zn, Si), which were not included in this study, 80–95% of PM 2.5 can be attributed to organic matter. The contribution of organic acids to PM 2.5 was of minor importance and showed only marginal differences between the three different seasons (Table 2c and Figure 1, bottom). The low seasonal variability of the organic acids may be related to the fact that they are associated with biogenic secondary organic aerosol (SOA) in addition to their pyrogenic sources. SOA are known to be a product of the photooxidation of volatile organic compounds (VOCs) that are emitted from the rain forest [see *Graham et al.*, 2003b, and references therein]. Organic acids are highly polar and may absorb water over the entire RH range [*Saxena and Hildemann*, 1997]. It should be noted that during LBA-EUSTACH-2 (1999) (biomass burning season), the overall sum of monocarboxylic, dicarboxylic, and polycarboxylic acids accounted for about 51% of the water-soluble organic carbon (WSOC) at the FNS site [*Mayol-Bracero et al.*, 2002].

3.2. Meteorological Conditions

[16] The average meteorological conditions during 12–23 September (dry season, biomass burning) at FNS are presented in Figures 2a–2d. Daytime (0900 to 1700 LT) wind speeds (Figure 2a) varied between 2 and 3 ms^{-1}. In contrast, nighttime wind speeds were very low, ranging from 0.5 to 1 m s^{-1}. This diel variation is a result of thermodynamic boundary layer characteristics observed frequently in the Amazon Basin [e.g., *Nobre et al.*, 1996; *Fisch et al.*, 2004]. Nighttime radiative cooling results in the formation of a shallow, nocturnal boundary layer of high thermodynamic stability and very low wind speeds. The growth of a convectively mixed layer starts with the heating of the surface in the morning. The daytime boundary layer is characterized by elevated wind speeds and strong turbulence. The wind direction (Figure 2b) showed a diel variation with winds mostly originating from the S-SE sector during daytime and from the W-SW sector during nighttime hours. This wind system was most likely orographically induced by the channeling effect of small hills near the FNS pasture site. During mid-afternoon (1400–1500 LT) winds typically came from the E-NE sector coinciding with the direction of the town Ouro Preto do Oeste.

[17] Ambient temperatures (Figure 2c) exhibited a regular and pronounced diel cycle with high values (33–36°C) between 1200 and 1500 LT, while during nighttime (2300–0700 LT) temperatures were below 25°C, dropping to 22°C between 0600 and 0700 LT. The diel variation of relative humidity (RH) at FNS revealed the opposite pattern; between 0430 LT and 0730 LT RH was close to 100%, and remained above 70% until 0900 LT. The noontime maximum of the global radiation flux (Figure 2d) reached 800–900 W m^{-2}. The variance of the radiation data was very low until 1030 LT and increased remarkably in the early afternoon: this indicates early morning clear sky conditions and the development of convective cloudiness and/or the presence of smoke plumes from 1100 LT onwards. According to the results of surface wetness measurements (Figure 2d), the grass canopy at FNS was covered by dew every night (2100 to 0730 LT). As soon as global radiation exceeded 200 W m^{-2} (0730 LT), dew layers evaporated within 1 hour and formed again when global radiation dropped below 100 W m^{-2} (1730 LT).

[18] The observed diel pattern of wind direction was diminished during the transition period (01–31 October) and the onset of the wet season (01–14 November). Through the transition period, characteristics of temperature

Table 2b. Average Mixing Ratios Plus or Minus Standard Deviation for Aerosol Na^+, K^+, Ca^{2+}, and Mg^{2+} (SFU Sampler, PM 2.5) During the Late Dry (Biomass Burning) Season (12–23 September), the Transition Period (7–31 October), and the Onset of the Wet Season (1–14 November) at FNS During LBA-SMOCC 2002

	Na^+, ppb	K^+, ppb	Ca^{2+}, ppb	Mg^{2+}, ppb
Dry season	0.016 ± 0.022	0.527 ± 0.180	0.152 ± 0.102	0.039 ± 0.029
Transition period	0.021 ± 0.017	0.106 ± 0.038	0.021 ± 0.015	0.011 ± 0.007
Wet season	0.028 ± 0.013	0.032 ± 0.007	0.017 ± 0.011	0.006 ± 0.003

Table 2c. Ranges of Measured Mono-/Di-/Tricarboxylic Acids, Aliphatic Oxo-/Hydroxyacids, and Aromatic Carboxylic Acids (SFU or HVDS Sampler, PM 2.5) During the Late Dry (Biomass Burning) Season (12–23 September), the Transition Period (7–31 October), and the Onset of the Wet Season (1–14 November) at FNS During LBA-SMOCC 2002

	Mono-/Di-/Tricarboxylic Acids, ppb	Aliphatic Oxo-/Hydroxyacids, ppb	Aromatic Carboxylic Acids, ppb
Dry season	0.003 to 0.133	0.003 to 0.066	0.008 to 0.021
Transition period	0.001 to 0.058	0.002 to 0.027	0.001 to 0.007
Wet season	below detection limit	below detection limit	below detection limit

and RH changed only marginally. However, minimum daytime RHs during the wet season were always above 55%. Correspondingly, maximal temperatures were 2 to 5°C lower than during the dry season. Strong rain events ($\geq$ 30 mm h^{-1}) occurred in the afternoon hours (1300 to 1600 LT) during the transition period and the wet season.

3.3. Diel Variations of Species Measured With the WAD/SJAC System

[19] Figures 3a–3h illustrate diel variations of the mixing ratios (median, 0.25 and 0.75 percentiles) of the trace gases NH_3, HNO_3, HCl, and SO_2, as well as of inorganic aerosol species NH_4^+, NO_3^-, Cl^-, and SO_4^{2-} (PM 2.5) during 12–23 September 2002 (dry season). Figure 3a shows a sharp spike of NH_3 mixing ratios just before 0900 LT. This feature is considered to be attributed to the strong decrease of surface wetness (Figure 2d), suggesting that NH_3 (most likely deposited and dissolved in epicuticular water films at nighttime) might evaporate in substantial amounts due to a temperature increase just after sunrise. This phenomenon was also observed in other studies [e.g., *Bussink et al.*, 1996; *Hesterberg et al.*, 1996]. During the same time period, an increase in aerosol NH_4^+ mixing ratio was observed (Figure 3b). At still high RH (70–80%, see Figure 2c) it is likely that a significant fraction of NH_3 has dissolved in humid aerosols, thereby enhancing aerosol NH_4^+. During the full expansion of the convective boundary layer after 0900 LT, surface air became more and more diluted by turbulent mixing with free tropospheric air, resulting in a decrease of NH_3 and aerosol NH_4^+. Although NH_3 and aerosol NH_4^+ mixing ratios decreased significantly during the transition period and especially in the wet period, their diel courses were similar.

[20] HNO_3 featured a typical diel cycle with high values at daytime and low values during the night (see Figure 3c). Daytime maxima of ~0.4 ppb (median) occurred in the early afternoon hours. This diel variation was mainly caused by (1) turbulent mixing from the free troposphere into the boundary layer during daytime, (2) daytime photochemistry (reaction of NO_2 with OH radical), (3) evaporation of HNO_3 from the aerosol phase at daytime (high T and low RH) (see Figure 2c), and (4) deposition of HNO_3 to wet vegetation elements at night [cf. *Trebs et al.*, 2004]. It should be noted that HNO_3 mixing ratios remained unexpectedly high during nighttime. Within a thermodynamically stable stratified nocturnal boundary layer, it is expected that the very sticky and water-soluble HNO_3 molecule will rapidly deposit to wet surfaces, which should be reflected by very low mixing ratios. The relatively high nighttime HNO_3 mixing ratios might be due to heterogeneous HNO_3 formation initiated by the reaction of NO_2 with O_3 [*Calvert et al.*, 1985]. In contrast, the median diel pattern of aerosol NO_3^- is characterized by high mixing ratios at night and low values during daytime (Figure 3d). Maximal mixing ratios occurred between 0000 and 0900 LT. Apparently, this was due to accumulation of NO_3^- in the aerosol phase under very humid conditions (Figure 2c) within a thermally stable nocturnal boundary layer. Lower RH during daytime may enable evaporation of NO_3^- from the aerosol phase leading to a decrease of corresponding mixing ratios (see section 3.4).

[21] The median diel pattern of HCl (Figure 3e) is comparable to that of HNO_3. However, nighttime mixing ratios of HCl were lower than corresponding HNO_3 mixing ratios. This suggests that, unlike HNO_3, HCl did not have significant chemical sources at nighttime, but its mixing ratios were largely depleted through deposition to wet grass surfaces. While mixing ratios of aerosol Cl^- were low (Figure 3f), they resembled the diel variations of aerosol NO_3^-, with the exception of a sharp peak of aerosol Cl^- around 1500 LT.

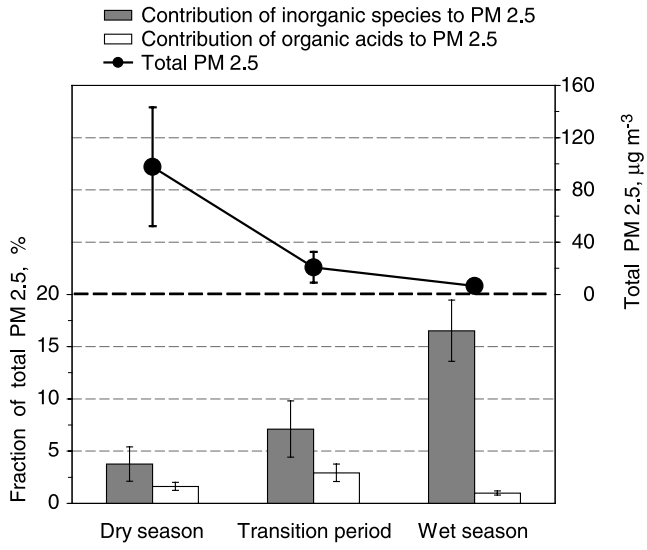

Figure 1. Average fine particulate mass (PM 2.5) (top), contribution of inorganic aerosol species to PM 2.5 (NH_4^+, NO_3^-, Cl^- and SO_4^{2-} measured by the WAD/SJAC system and Na^+, K^+, Ca^{2+}, Mg^{2+} measured by the SFU sampler) and contribution of organic acids (the sum of species considered in this study measured by SFU and HVDS sampler) to PM 2.5 (bottom) for the late dry (biomass burning) season, transition period and the onset of the wet season at FNS during LBA-SMOCC 2002 (error bars indicate standard deviations of averages).

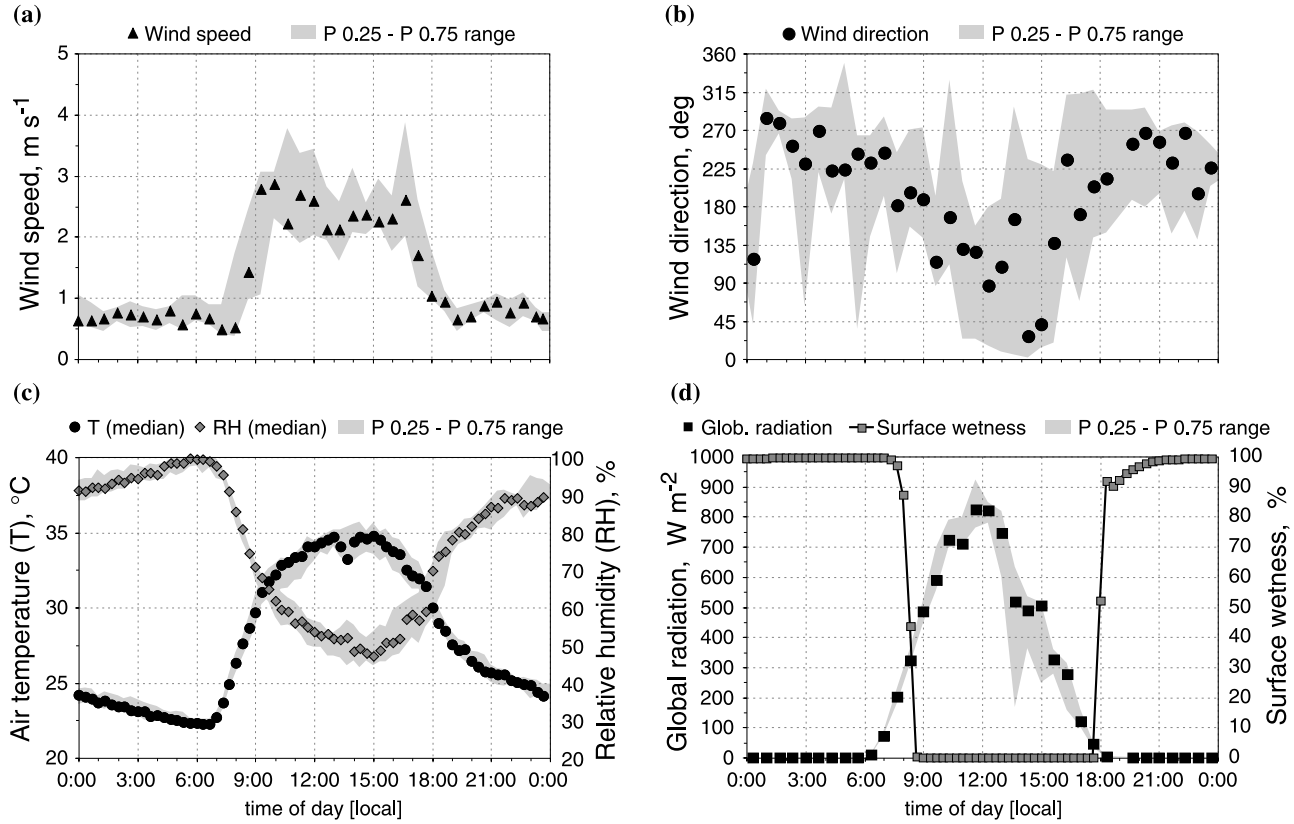

Figure 2. Diel variations of (a) wind speed, (b) wind direction, (c) air temperature (T) and relative humidity (RH), and (d) global radiation flux and surface wetness during 12–23 September 2002 (dry season, biomass burning) at FNS during LBA-SMOCC 2002. Symbols and grey shading represent medians and interquartile ranges (0.25 to 0.75 percentiles), respectively.

[22] SO_2 generally showed higher mixing ratios at daytime (Figure 3g) and the diel course of aerosol SO_4^{2-} was characterized by relatively constant mixing ratios, except for the period 1100 to 1300 LT (Figure 3h). Aerosol SO_4^{2-} is known to be nonvolatile, and timescales for its chemical formation (photo-chemical oxidation of SO_2) are large [*Calvert et al.*, 1985]. Therefore, the diel cycle of aerosol SO_4^{2-} broadly reflects advection of air masses.

[23] The 1100–1300 LT minimum of aerosol SO_4^{2-} coincides with minima of gaseous SO_2, aerosol Cl^-, NO_3^-, and NH_4^+. Around noon, convective mixing, high T and low RH (see Figure 2c) generally resulted in lower mixing ratios of aerosol species. Around 1500 LT distinctively higher mixing ratios of gaseous SO_2 and aerosol Cl^-, and also somewhat higher values of aerosol NH_4^+ and NO_3^- and SO_4^{2-} were observed. This is the only time of the day when winds arrived from E–NE; carrying pollutants from the town Ouro Preto do Oeste to the site.

[24] Except for NH_3 and aerosol NH_4^+, the diel courses of gas and aerosol phase mixing ratios were less pronounced during the transition period. Generally, diel fluctuations were diminished under cleaner conditions during the onset of the wet season.

3.4. Gas/Aerosol Relationships

[25] The FNS site can be characterized as an NH_3-rich environment (see Table 2a). The ratio of NH_3 to SO_2 mostly exceeded a value of 10, reaching values up to 100. The average ratio of aerosol NH_4^+/SO_4^{2-} was 4.4. High levels of NH_3 are attributed to emissions from cattle manure and to biomass burning during the dry season [*Trebs et al.*, 2004]. Human activities in this region do not appear to be strong sources of SO_2. The transfer of HCl and HNO_3 from the gas to the aerosol phase is generally controlled by the neutralization of H_2SO_4 with NH_3. Due to the large excess of NH_3 vapor pressure over that of HNO_3, HCl and SO_2 at FNS, chemical limitations for the transfer of HCl and HNO_3 to the aerosol phase are very unlikely. Figure 4 emphasizes that $(NH_4)_2SO_4$ formation is favored over that of NH_4NO_3, which implies that NH_4NO_3 is assumed to be formed only when H_2SO_4 is already consumed and NH_3 mixing ratios are still high. However, because of the limited H_2SO_4 and HNO_3 availability at the FNS site, excess NH_3 is expected to be largely neutralized by other acidic species. This will be investigated in detail below.

[26] Gas/aerosol partitioning coefficients (ratios aerosol/(gas + aerosol)) for ammonium, nitrate and chloride are shown in Figures 5a–5f. Although the diel course of the NH_4^+ partitioning coefficient (Figure 5a) is not very pronounced, the fraction of aerosol NH_4^+ was slightly higher at night (0.4–0.5) and lower during daytime (0.2–0.3). The fraction of aerosol NH_4^+ started to increase at RH > 80% (Figure 5b). In contrast, NO_3^- and Cl^- partitioning coefficients exhibited a remarkable dependence on RH (see Figures 5d and 5f). The patterns of median diel cycles shown in Figures 5c and 5e closely resemble that of RH

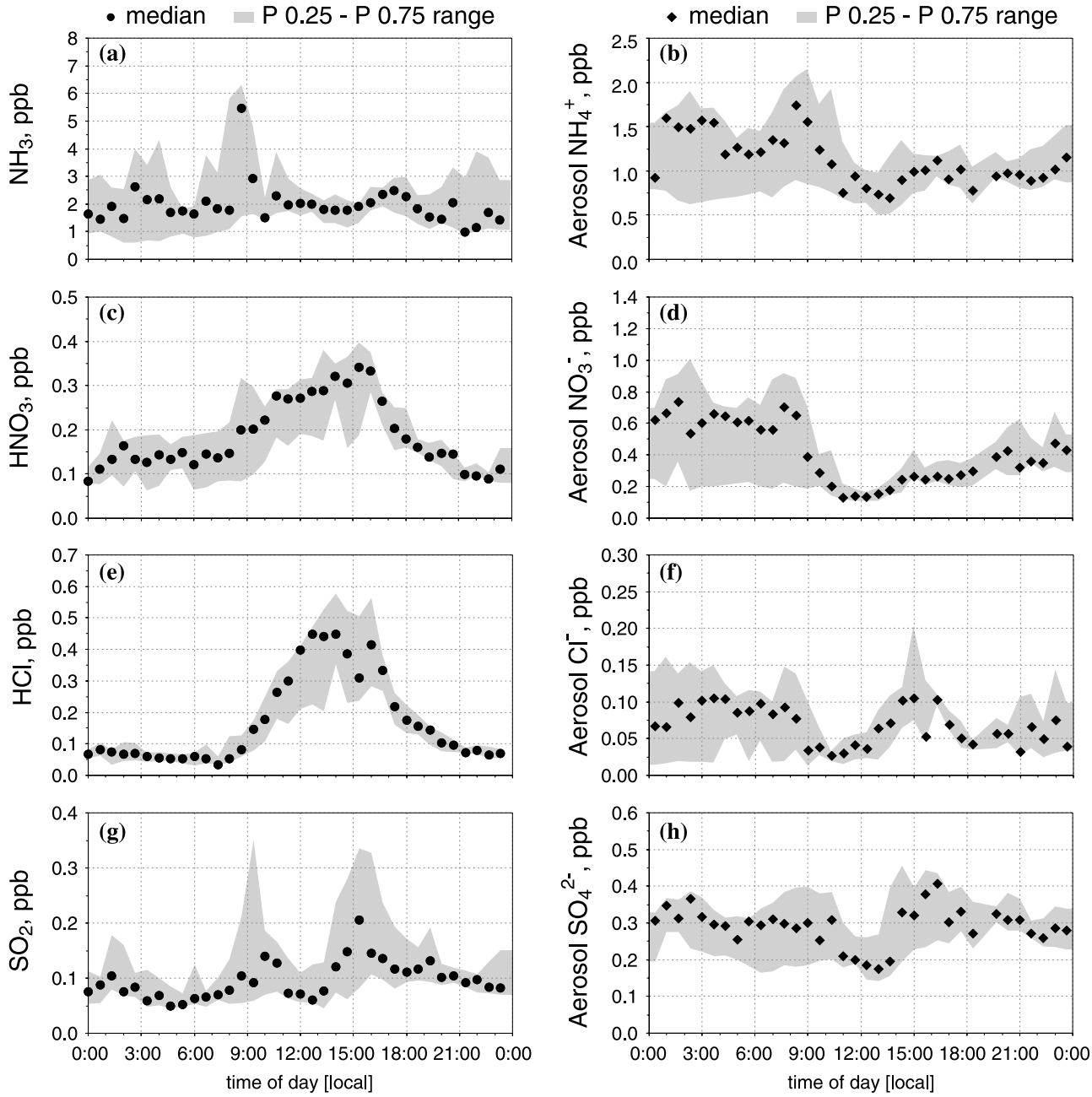

Figure 3. Diel variations of (a) NH_3, (b) aerosol NH_4^+ (PM 2.5), (c) HNO_3, (d) aerosol NO_3^- (PM 2.5), (e) HCl, (f) aerosol Cl^- (PM 2.5), (g) SO_2, and (h) aerosol SO_4^{2-} (PM 2.5) measured with the WAD/SJAC system during 12–23 September 2002 (dry season, biomass burning) at FNS during LBA-SMOCC 2002. Symbols and grey shading represent medians and interquartile ranges (0.25 to 0.75 percentiles), respectively.

(Figure 2c). At nighttime, 80% of the total NO_3^- was present in the aerosol phase. During daytime 60% of the total NO_3^- was attributed to gaseous HNO_3. A comparable behavior was found for Cl^-, although the fraction of aerosol Cl^- was lower than that observed for NO_3^-. At nighttime the maximum aerosol Cl^- fraction was only 0.4–0.5, decreasing to <0.2 at daytime. Nevertheless, the difference of aerosol associated NO_3^- and Cl^- between day and night was identical (2- fold increase from day to nighttime). The higher NO_3^- aerosol fraction was most likely due to the strong tendency of HNO_3 to absorb on wet surfaces and subsequent uptake by the liquid phase. A similar finding was reported by *Mehlmann and Warneck* [1995], who showed that 95% of the total NO_3^- was present in the aerosol phase at RH = 85%.

[27] It should be emphasized that the graphs in Figures 5a–5f were compiled including measurements from the late dry season, transition period and the onset of the wet season. Despite a strong decrease in the observed mixing ratios from the dry to the wet season, interquartile ranges and standard deviations in Figures 5a–5f are small. Obviously, partitioning of inorganic species between gas

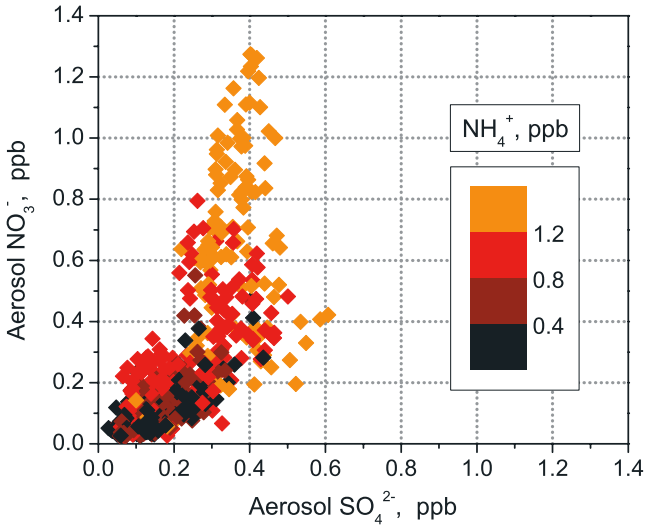

Figure 4. Aerosol NO_3^- versus SO_4^{2-} at different aerosol NH_4^+ mixing ratios (color coded) at FNS during LBA-SMOCC 2002. Results obtained with the WAD/SJAC system from all three seasons were combined (n = 528).

and aerosol phase at FNS is strongly controlled by ambient RH, regardless of season. Figures 5a–5f would reveal the opposite pattern for the temperature dependence of the partitioning coefficients, indicating that low temperatures favor condensation of gaseous compounds and high temperatures cause evaporation of semivolatile species from aerosol particles.

4. Discussion

[28] In order to explain the results presented above and to gain further insights into the complex gas/aerosol system at this tropical site, the aerosol ion balance and gas/aerosol partitioning processes will be discussed in the following sections. For the latter, thermodynamic theory is considered with the aid of four different EQMs.

4.1. Charge Balance of Ionic Aerosol Species

[29] Electrical charge balances of the observed ionic aerosol components are a useful tool to test the accuracy of measurements and to judge on missing anions or cations. The ion balance presented in Figure 6a considers only the ions measured with the WAD/SJAC system (NH_4^+, NO_3^-, Cl^-, and SO_4^{2-}, PM 2.5). The error bars represent measurement uncertainties determined by Gaussian error propagation based on results from *Trebs et al.* [2004]. The mean uncertainty is ~8% for the sum of anions (NO_3^-, Cl^- and SO_4^{2-}) and ~14% for NH_4^+. NH_4^+ correlates well with the sum of NO_3^-, Cl^- and SO_4^{2-} equivalents (r^2 = 0.67, n = 260). The median cation/anion ratio for this case was 1.20 (P 0.25 = 0.99 and P 0.75 = 1.46) suggesting that there is abundant NH_3 to neutralize HNO_3, HCl and H_2SO_4. However, it can be argued that ~ 20% of the NH_4^+ present in the sampled fine mode aerosols must be balanced by additional counter ions that were not measured by the WAD/SJAC system.

[30] In order to complete the ion balance, data obtained from the SFU and HVDS samplers (PM 2.5) are included (Figures 6b and 6c). To allow for comparison of samples collected with different time resolutions, we assumed constant ambient mixing ratios determined on 12-, 24-, and 48-hours integrated filter samples. Filter data were assigned to the corresponding data points obtained with the WAD/SJAC system every 20-, 40-, and 60-min during the respective 12-, 24-, and 48-hour interval. The inclusion of additional cations (Na^+, K^+, Ca^{2+} and Mg^{2+}) as shown in Figure 6b, results in a significant shift of the charge balance away from the 1:1 relationship. For this case, the mean measurement uncertainty (error bars in Figure 6b) is ~8% for the sum of anions and ~10% for the sum of cations. The median cation/anion ratio is now 2.18 (P 0.25 = 1.69 and P 0.75 = 2.96), strengthening the hypothesis that additional anions are necessary to balance aerosol cationic charges. This significant shift was primarily caused by the high abundance of K^+ in the fine mode aerosol (see Table 2b), which is directly emitted by biomass fires and vegetation in this region [*Allen and Miguel*, 1995; *Yamasoe et al.*, 2000, and references therein]. *Kerminen et al.* [2001] and *Lee et al.* [2003] proposed that the presence of water-soluble organic anions may be of importance for the aerosol charge balance. Due to the high mixing ratios of gaseous NH_3 at our sampling site (see Table 2a) sufficient alkaline material to neutralize (deprotonate) organic acidic aerosol species (shown in Table 2c) may be provided:

$$NH_3 + \text{R-COOH} \rightarrow \text{R-COO}^- + NH_4^+$$

[31] The organic compounds included here belong to the group of the weak acids. As a first approximation, equivalent moles were calculated assuming that mono-, di-, and tricarboxylic acids form the respective mono-, di-, and triammonium salts, which means they may donate all H^+ to neutralize NH_3. Since the pH of the sampled aerosol is not known, it is difficult to estimate the degree of acid dissociation, but we may speculate that full acid dissociation occurred due to the excess of NH_3 available at the site. In Figure 6c organic acids are added to the ionic charge balance accounting for the total of carboxylic groups. The mean measurement uncertainty (error bars in Figure 6c) determined by Gaussian error propagation for anions including organic acids is ~10%. The median cation/anion ratio for this case is 1.06 (P 0.25 = 0.90 and P 0.75 = 1.31), approaching a 1:1 ratio of cationic and anionic charges (r^2 = 0.67, n = 260). The remaining discrepancy between the measured anionic and cationic charges is only ~6%. However, assuming that only mono-ammonium salts form from all carboxylic acids (except oxalic acid), this discrepancy increases to ~27%. It has to be considered here that the sum of cationic and anionic charges is not complete. Species that are not detectable by the methods applied, such as H^+, OH^- and CO_3^{2-} might influence the charge balances shown here. Also, most likely not all of the LMW polar organic acids present in the sampled aerosol could be detected by our techniques, and such undetected species may play a role in the charge balance.

[32] *Graham et al.* [2003a] found a reasonably good ion balance for fine mode Amazonian aerosols measured with integrating filter samplers during the wet season when only inorganic ions and oxalate were included. However, for the

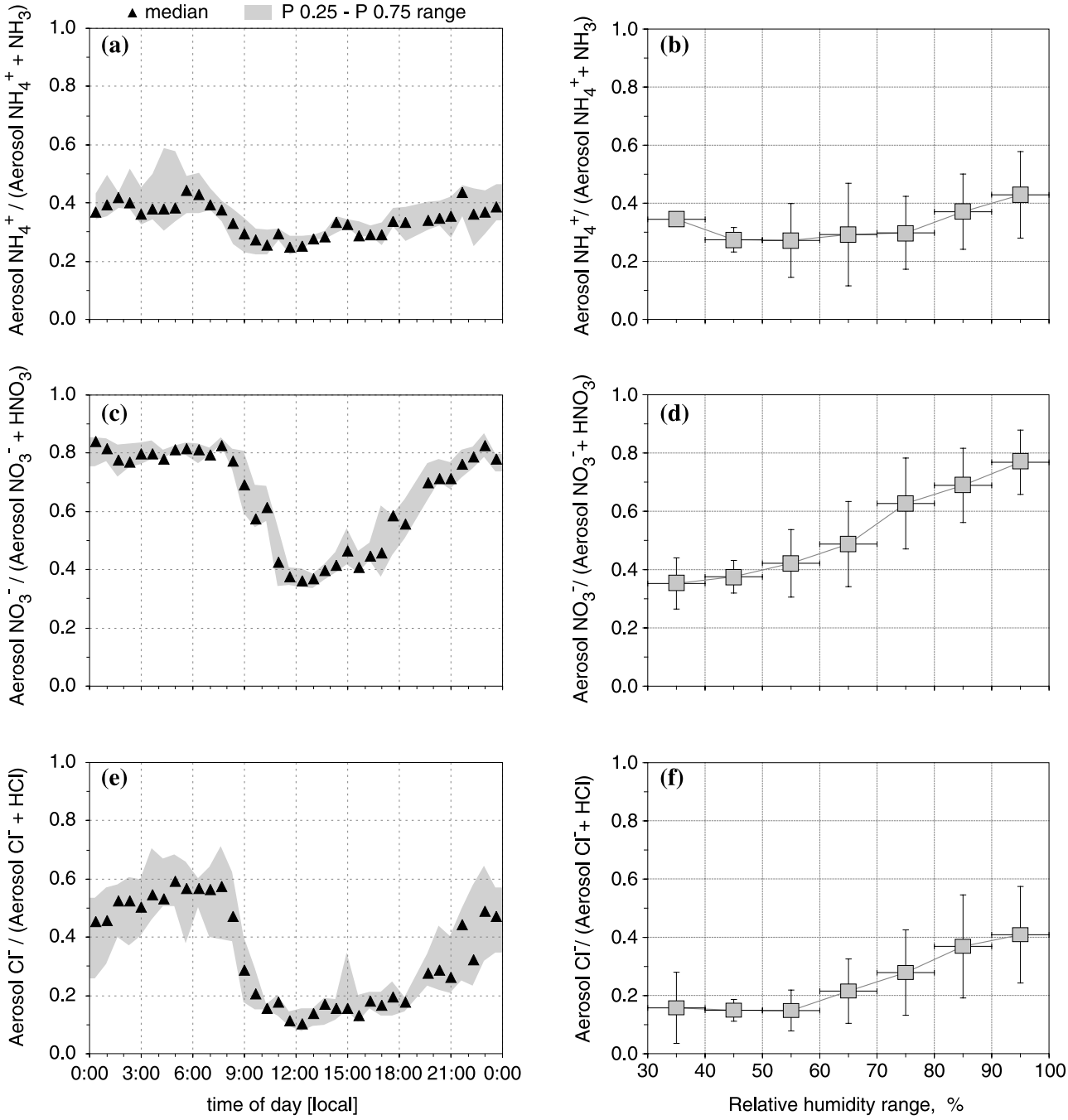

Figure 5. (a) Diel variation of aerosol NH_4^+/total NH_4^+ (n = 508), (b) RH dependence of aerosol NH_4^+/total NH_4^+ (n = 508), (c) diel variation of aerosol NO_3^-/total NO_3^- (n = 483), (d) RH dependence of aerosol NO_3^-/total NO_3^- (n = 483), (e) diel variation of aerosol Cl^-/total Cl^- (n = 570), and (f) RH dependence of aerosol Cl^-/total Cl^- (n = 570). For Figures 5a, 5c, and 5e, symbols and grey shading represent medians and interquartile ranges (0.25 to 0.75 percentiles), respectively. For Figures 5b, 5d, and 5f, y-error bars represent standard deviations of average ratios, and x-error bars indicate RH range. Results obtained with the WAD/SJAC system from all three seasons at FNS during LBA-SMOCC 2002 were combined.

coarse aerosol fraction they observed anion deficits that were probably attributed to additional organic anions. Likewise, previous studies using filter techniques suggested that the Amazonian dry season aerosol is acid-base neutral when inorganic ions and oxalic, acetic and formic acid are included in the charge balance [*Talbot et al.*, 1988].

[33] Nevertheless, in our study we combined results of fine mode aerosol NH_4^+, NO_3^-, Cl^- and SO_4^{2-} (measured with a real-time method, not prone to artifacts [cf. *Trebs et al.*, 2004]) with results of Na^+, K^+, Ca^{2+} and Mg^{2+} and organic aerosol species (from integrating filter samplers) to determine the aerosol charge balance. The results suggest

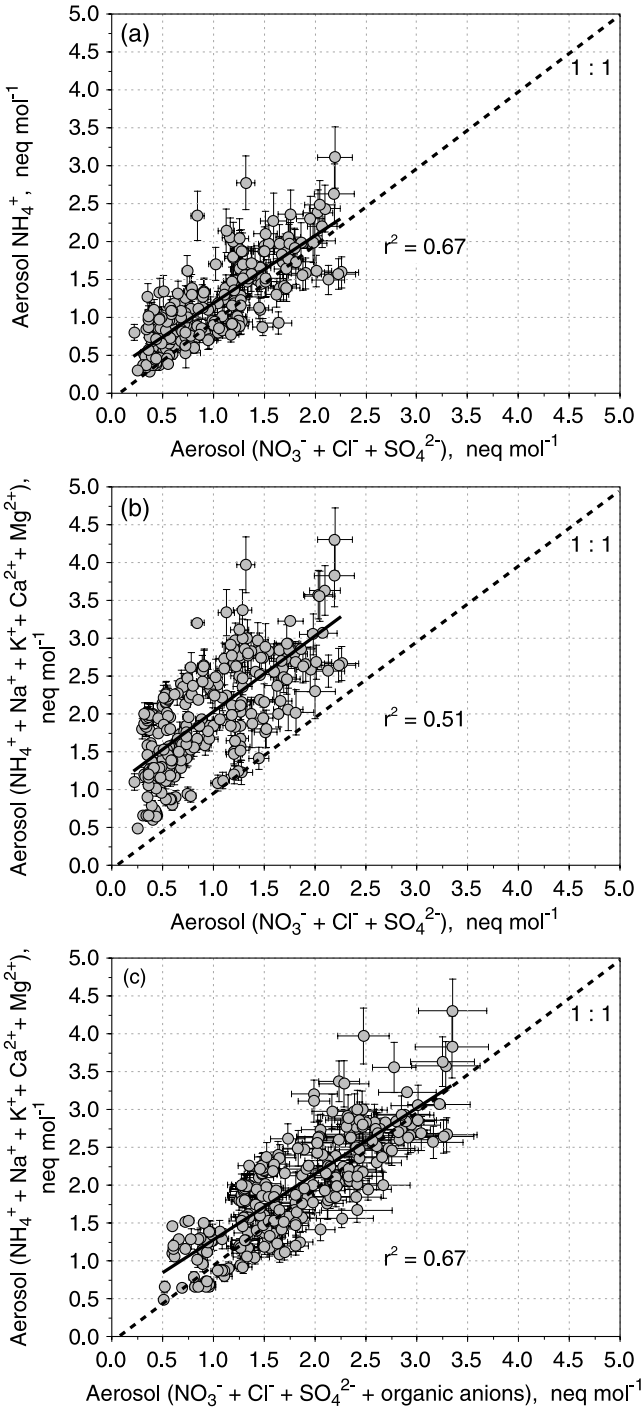

Figure 6. Balances between anionic and cationic charges of the aerosol fine fraction (PM 2.5) sampled at FNS during SMOCC 2002 (n = 260): (a) balance for anions and cations measured with the WAD/SJAC system, (b) same as Figure 6a, but cation data (Na^+, K^+, Ca^{2+}, and Mg^{2+}) from the SFU sampler are included, and (c) same as Figure 6b, but the sum of organic anions obtained from SFU and HVDS samplers are included (error bars represent measurements uncertainties for anions and cations, see text).

that, LMW organic acids besides oxalate, acetate and formate contribute significantly to the charge balance of Amazonian fine mode aerosols. Due to the inclusion of organic acids into the inorganic aerosol ion balance the discrepancy of 100% (factor 2) between anionic and cationic charges (see Figure 6b) could be reduced by at least a factor of three to 6–27% (Figure 6c).

4.2. Thermodynamic Equilibrium Assumption at FNS

[34] Following similar studies on equilibria of inorganic trace gases with related ionic aerosol compounds, we have tested if thermodynamic equilibrium was attained for the pure $NH_3/HNO_3/NH_4NO_3$ and $NH_3/HCl/NH_4Cl$ systems under the meteorological conditions prevailing at FNS. The theoretical equilibrium dissociation constant is computed and compared to the measured concentration products of NH_3 & HNO_3 and NH_3 & HCl. In Figure 7a, the thermodynamically predicted equilibrium dissociation constant (K_e) for pure NH_4NO_3 and the measured concentration product (K_m = HNO_3 × NH_3) are shown as a function of RH. Liquid phase equilibria of nonideal solutions are based on the application of a theoretically derived formulation of solution molalities and activity coefficients according to *Metzger et al.* [2002]. For typical mean ambient temperatures of 25–28°C at the sampling site (see Figure 2c) the measured concentration product (K_m = HNO_3 × NH_3) is always 1 to 2 orders of magnitude below K_e for RH < 90%. K_m approaches K_e at RH > 90% and lower temperatures (nighttime).

[35] The coincidence of high RH and high temperatures prevailing in the Amazon Basin is not very common in temperate latitudes, where previous studies have been conducted, which makes comparisons difficult. In contrast to our work, these studies showed that large differences between K_m and K_e for pure NH_4NO_3 at RH < 90% are not common. *Tanner* [1980], *Erisman et al.* [1988], and *Harrison and Msibi* [1994] reported a good agreement of predicted K_e with K_m for temperatures of 0–20 °C and RH < 80%. A study by *Harrison and Pio* [1983] showed that at T < 10°C and RH > 60% equilibrium was achieved. In contrast, *Cadle et al.* [1982] and *Allen et al.* [1989] reported that at low temperatures or high RH the equilibrium condition is not met. It was confirmed by *Matsumoto and Tanaka* [1996], *Danalatos and Glavas* [1999], *Parmar et al.* [2001], and *Gupta et al.* [2003] that lower temperatures generally favor formation of NH_4NO_3 and that at higher temperatures gas/aerosol equilibrium is not achieved, which might explain the large deviations of K_m to K_e in our study.

[36] Deviations from equilibrium may be due to (1) measurement artifacts, especially at long sampling times, (2) HNO_3 deposition faster than attainment of equilibrium, (3) mass transport limitations and kinetic constraints [*Wexler and Seinfeld*, 1992], particularly under highly polluted conditions or in case of freshly emitted NH_3 and HNO_3, (4) long equilibration times due to the presence of large particles (equilibration times for coarse mode aerosols are usually longer than for fine mode particles [*Meng and Seinfeld*, 1996]), and (5) formation of nonvolatile NO_3^- salts by reaction of HNO_3 with sea salt or soil dust [*Hildemann et al.*, 1984; *Parmar et al.*, 2001].

[37] For deliquescent aerosol particles, the coexistence of SO_4^{2-} considerably reduces K_e compared to pure NH_4NO_3

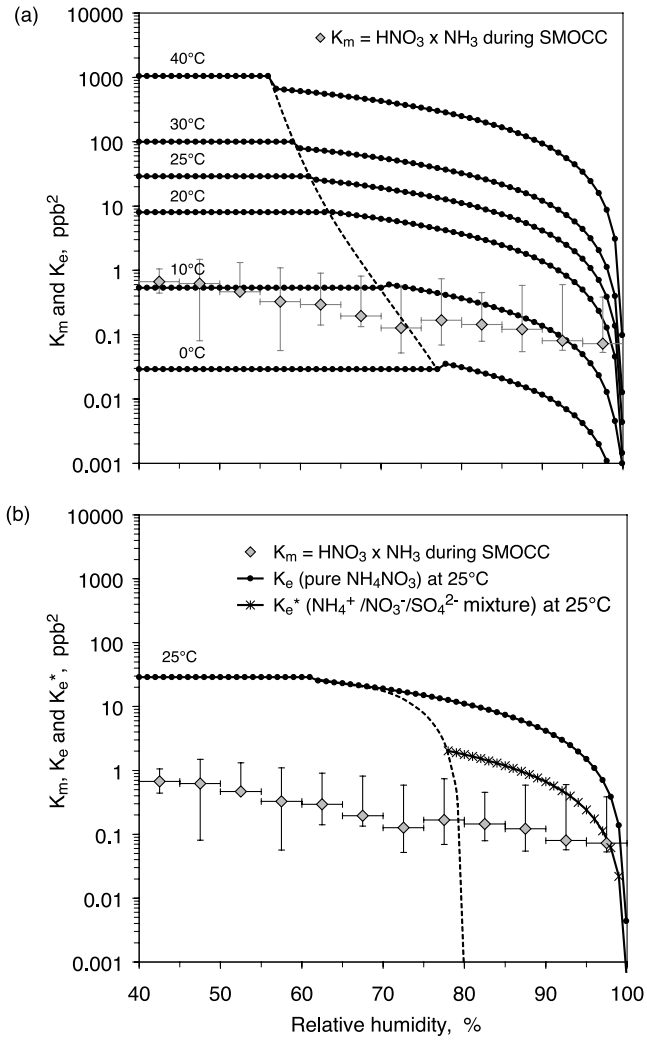

Figure 7. Thermodynamically predicted equilibrium dissociation constant (K_e) for (a) pure NH_4NO_3, and (b) NH_4^+/NO_3^-/SO_4^{2-} mixtures at 25°C (K_e*) in comparison to averages of the measured concentration product (K_m = HNO_3 × NH_3) as a function of RH at FNS during LBA-SMOCC 2002 (including data from the late dry season, transition period and the onset of the wet season, n = 474); y-error bars indicate standard deviations of averages, x-error bars indicate the RH bin used for averaging; the dashed line indicates the transition from solid to nonideal aqueous solution (adapted from *Stelson and Seinfeld* [1982a, 1982b]).

solutions [*Stelson and Seinfeld*, 1982b]. To determine K_e^* for the $NH_4^+/NO_3^-/SO_4^{2-}$ system, the NH_4NO_3 ionic strength fraction Y is calculated according to [*Stelson and Seinfeld*, 1982b]:

$$Y = \frac{[NH_4NO_3]}{[NH_4NO_3] + 3[(NH_4)_2SO_4]}$$

resulting in a median value of Y = 0.16. K_e^* was then derived by multiplying K_e with Y, which resulted in a K_e^* value that was significantly lower than K_e at 25°C (Figure 7b). Although for RH > 90% K_m is nearly equal to K_e^*, K_m remains below K_e^* for RH < 90%. These findings might suggest that at the high temperatures prevailing at the FNS site the vapor pressures of NH_3 and HNO_3 were too low to allow formation of NH_4NO_3 at RH < 90%.

[38] Since HCl is more volatile than HNO_3 [*Matsumoto and Tanaka*, 1996], K_e for the $NH_3/HCl/NH_4Cl$ system is somewhat higher than the theoretical value for the pure $NH_3/HNO_3/NH_4NO_3$ system (illustrated in *Allen et al.* [1989]). The HCl vapor pressures and diel variations measured at the site were comparable to those observed for HNO_3 (see Figures 3c and 3e and Table 2a), thus K_m for the $NH_3/HCl/NH_4Cl$ system exhibits a similar behavior to K_m shown in Figure 7a (i.e., $K_m < K_e$ for RH < 90%). Nevertheless, aerosol NH_4^+, NO_3^- and Cl^- were observed at FNS over the entire RH range (40–100%), in disagreement with the thermodynamic equilibrium prediction for RH < 90%.

4.3. Equilibrium Model (EQM) Simulations

[39] The theoretical considerations above are restricted to the $NH_3/HNO_3/NH_4NO_3$ and $NH_3/HCl/NH_4Cl$ systems; thus, they may not entirely explain ionic balances, gas/aerosol partitioning and formation processes of inorganic aerosol constituents at FNS. Therefore, in this section, we will apply four EQMs that are capable of simulating a comprehensive multicomponent inorganic gas/liquid/solid aerosol system.

[40] The input parameters for EQSAM2, ISORROPIA, GEFMN, and SCAPE2 are ambient temperature, RH, total NH_4^+, total NO_3^-, total Cl^-, aerosol SO_4^{2-}, aerosol Na^+, and, if required, aerosol mineral cations (K^+, Ca^{2+}, Mg^{2+}) and LMW polar organic acids (only for EQSAM2). Model simulations were based on gas/liquid/solid partitioning considering all physical states of the aerosol (solid/deliquescence/efflorescence). For the GEFMN model, thermodynamic data are not valid for RH > 94%, thus RHs higher than 94% were set equal to 94% for all GEFMN runs. Our investigations focus on a period in the dry season (biomass burning, 17–20 September 2002; PM 2.5). Model results will be discussed for the following three gas/liquid/solid aerosol systems: (1) Na^+-HCl/Cl^--NH_3/NH_4^+-HNO_3/NO_3^--H_2SO_4/SO_4^{2-}-H_2O; (2) K^+-Ca^{2+}-Mg^{2+}-Na^+-HCl/Cl^--NH_3/NH_4^+-HNO_3/NO_3^--H_2SO_4/SO_4^{2-}-H_2O; (3) K^+-Ca^{2+}-Mg^{2+}-Na^+-HCl/Cl^--NH_3/NH_4^+-HNO_3/NO_3^--H_2SO_4/SO_4^{2-}-H_2O including lumped LMW polar organic acids (only EQSAM2).

[41] Since SCAPE2 and EQSAM2 are the only EQMs that consider mineral cations in their modeling framework, these compounds are represented in ISORROPIA and GEFMN as equivalent mixing ratio of Na^+. The implicit inclusion of mineral cations as Na^+ equivalent was applied before by *Moya et al.* [2001], who showed that ISORROPIA performs almost as well as SCAPE2 when using this approach. However, since the distinct behavior of mineral solid phase equilibria can not be resolved ($MgCl_2$ deliquesces already at RH ~ 33% (298.15 K) and NaCl at RH ~ 75% (298.15 K)), this approach is limited to gas/liquid equilibria and will lead to a considerable underestimation of the aerosol water content. Therefore, we will use SCAPE2 from now on as the reference model.

[42] Plots of modeled aerosol SO_4^{2-} will not be presented here, since aerosol SO_4^{2-} is nonvolatile and H_2SO_4 is fully

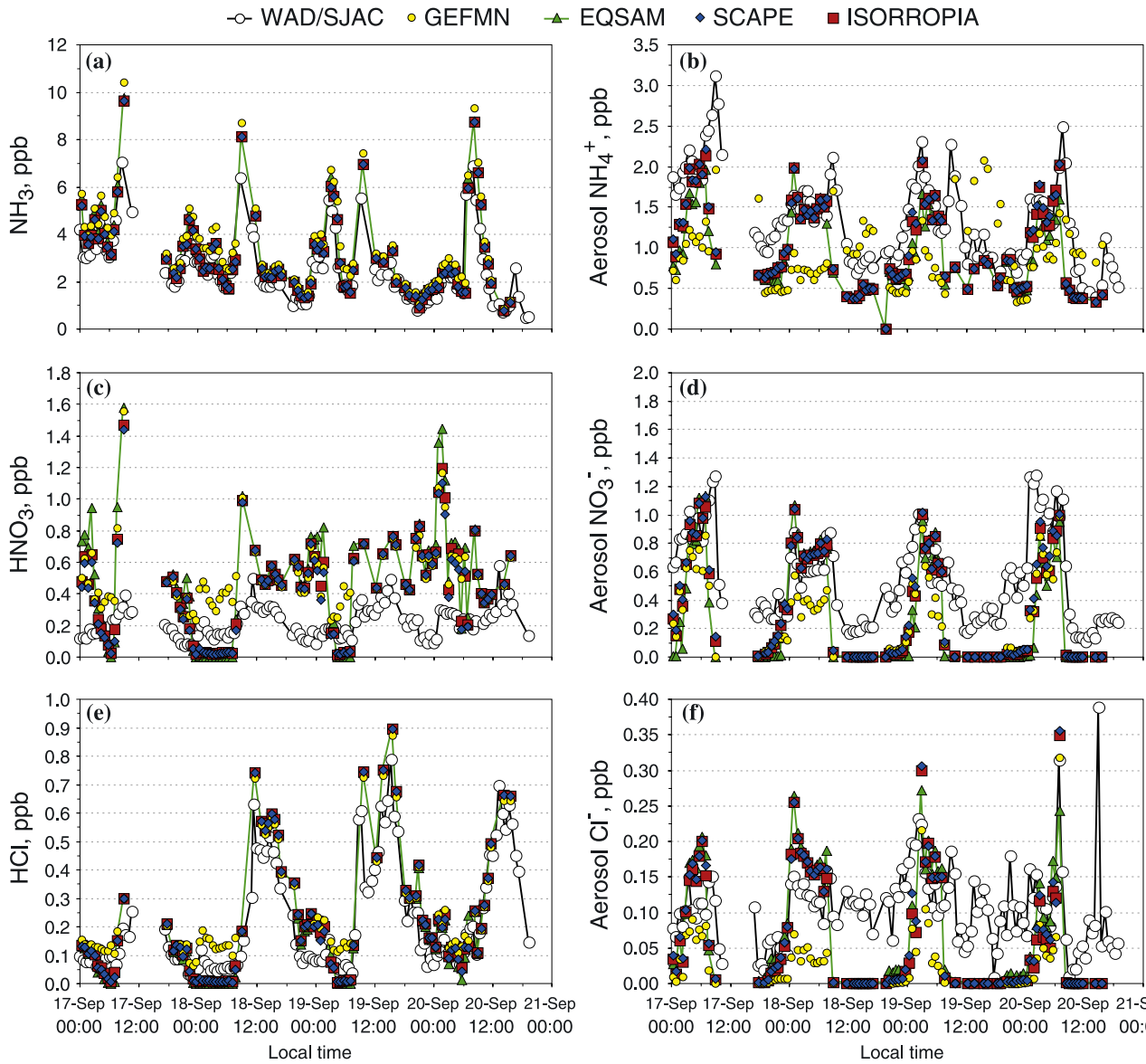

Figure 8. Diel variations of (a) NH_3, (b) aerosol NH_4^+, (c) HNO_3, (d) aerosol NO_3^-, (e) HCl, and (f) aerosol Cl^- measured with the WAD/SJAC system (PM 2.5) along with results of simulations with EQSAM2, ISORROPIA, GEFMN, and SCAPE2 for the Na^+-HCl/Cl^--NH_3/NH_4^+-HNO_3/NO_3^--H_2SO_4/SO_4^{2-}-H_2O-system, 17–20 September 2002, dry (biomass burning) season at FNS during LBA-SMOCC 2002.

neutralized in all cases. Therefore, mixing ratios of aerosol SO_4^{2-} remain the same as in the model input which corresponds to the measured values (shown for 17–20 September 2002 in *Trebs et al.* [2004]).

4.3.1. Na^+-HCl/Cl^--NH_3/NH_4^+-HNO_3/NO_3^--H_2SO_4/SO_4^{2-}-H_2O-System

[43] Figures 8a–8f show diel variations of inorganic compounds measured with the WAD/SJAC system along with the simulated values from the four EQMs for a system including only NH_3/NH_4^+, HNO_3/NO_3^-, HCl/Cl^-, H_2SO_4/SO_4^{2-}, and aerosol Na^+ (17–20 September 2002). Generally, the models overpredict gaseous compounds and underpredict inorganic aerosol species. Obviously, during daytime hours coinciding with lower RH (Figure 2c), the EQMs fail to predict the existence of the observed aerosol NO_3^- and Cl^-, leading to a significant overprediction especially of HNO_3, but also HCl (Figures 8c and 8e). As a result, only the amount of NH_3 required for the neutralization of H_2SO_4 is simulated as NH_4^+ in the aerosol phase during daytime. In contrast, modeled inorganic aerosol species are much closer to the observations during nighttime. This finding is emphasized in Figure 9; while the WAD/SJAC measurements showed detectable fine mode aerosol NO_3^- that was increasing with increasing RH, SCAPE2 does not predict any aerosol NO_3^- at RH < 90%. For RH > 90% SCAPE2 simulates aerosol NO_3^- in reasonable agreement with the measurements. Model predictions of fine mode aerosol Cl^- are comparable to the findings for aerosol NO_3^-. Simulated values are lower than observations even at RH > 90% (not shown). In summary, the EQM simulations suggest that

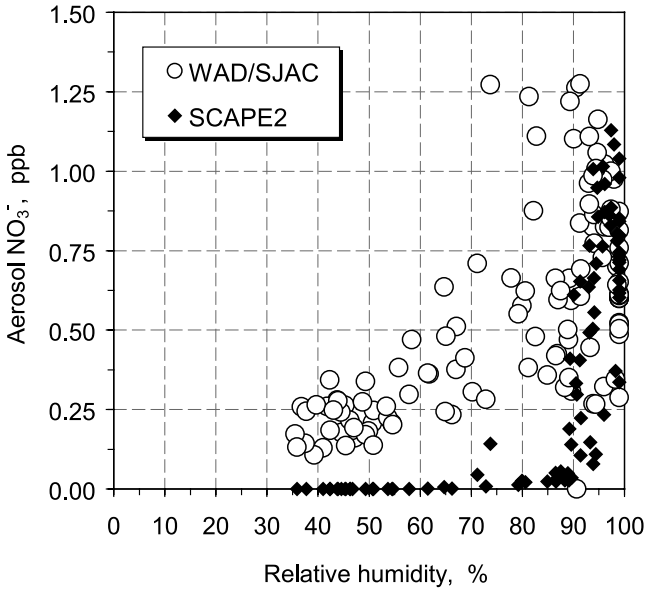

Figure 9. Relative humidity dependence of measured aerosol NO_3^- (PM 2.5) and SCAPE2 predicted aerosol NO_3^- for the Na^+-HCl/Cl^--NH_3/NH_4^+-HNO_3/NO_3^--H_2SO_4/SO_4^{2-}-H_2O-system, 17–20 September 2002, dry (biomass burning) season at FNS during LBA-SMOCC 2002.

thermodynamic equilibrium between NH_3, HNO_3, HCl and aerosol NH_4NO_3 and NH_4Cl does not adequately represent the observed phase relationships for RH < 90%, and that other components must be considered to explain the differences between observations and model results.

4.3.2. K^+-Ca^{2+}-Mg^{2+}-Na^+-HCl/Cl^--NH_3/NH_4^+-HNO_3/NO_3^--H_2SO_4/SO_4^{2-}-H_2O-System

[44] In order to assess the role of the mineral cations (K^+, Ca^{2+}, Mg^{2+}) we will now investigate a system consisting of NH_3/NH_4^+, HNO_3/NO_3^-, HCl/Cl^-, H_2SO_4/SO_4^{2-}, aerosol Na^+, aerosol K^+, aerosol Ca^{2+}, and aerosol Mg^{2+}. Figure 10a shows that, when mineral cations are included, aerosol NO_3^- is predicted by SCAPE2 also at RH < 90%. Apparently, besides the presence of NH_4NO_3 at RH > 90%, a sizeable fraction of NO_3^- was balanced by mineral cations (predominantly K^+, which was most abundant in the aerosol fine mode, see Table 2b). According to the SCAPE2 simulations, daytime fine mode aerosol NO_3^- may solely be attributed to nonvolatile nitrate salts, which were probably formed through heterogeneous uptake of HNO_3 by aerosol particles. Thus, once aqueous NH_4NO_3 has evaporated due to decreasing RH at sunrise (see Figures 2c and 2d), only the amount of fine mode NO_3^- balanced by mineral cations remained in the aerosol phase at lower daytime RHs. However, SCAPE2 somewhat overpredicts aerosol NO_3^- at RH < 60% (see Figure 10a). This may be caused by the fact that real-time measurements are combined with results from 12, 24 and 48 hours integrating filter samplers, which do not represent the diel variability of mineral cations. On the other hand, it is possible that aerosol NO_3^- did not achieve equilibrium with mineral cations because of transport limitations (mass transport of species between gas and aerosol phase is not considered in SCAPE2 and other EQM frameworks). Modeled fine mode aerosol Cl^- repeatedly shows a similar behavior to aerosol NO_3^- and is also predicted by SCAPE2 at RH < 90% when mineral cations are included (not shown). It may be assumed that aerosol Cl^- behaved similarly to aerosol NO_3^-, mainly because it was balanced by mineral cations at daytime while a considerable fraction was present as aqueous NH_4Cl at high nighttime RHs.

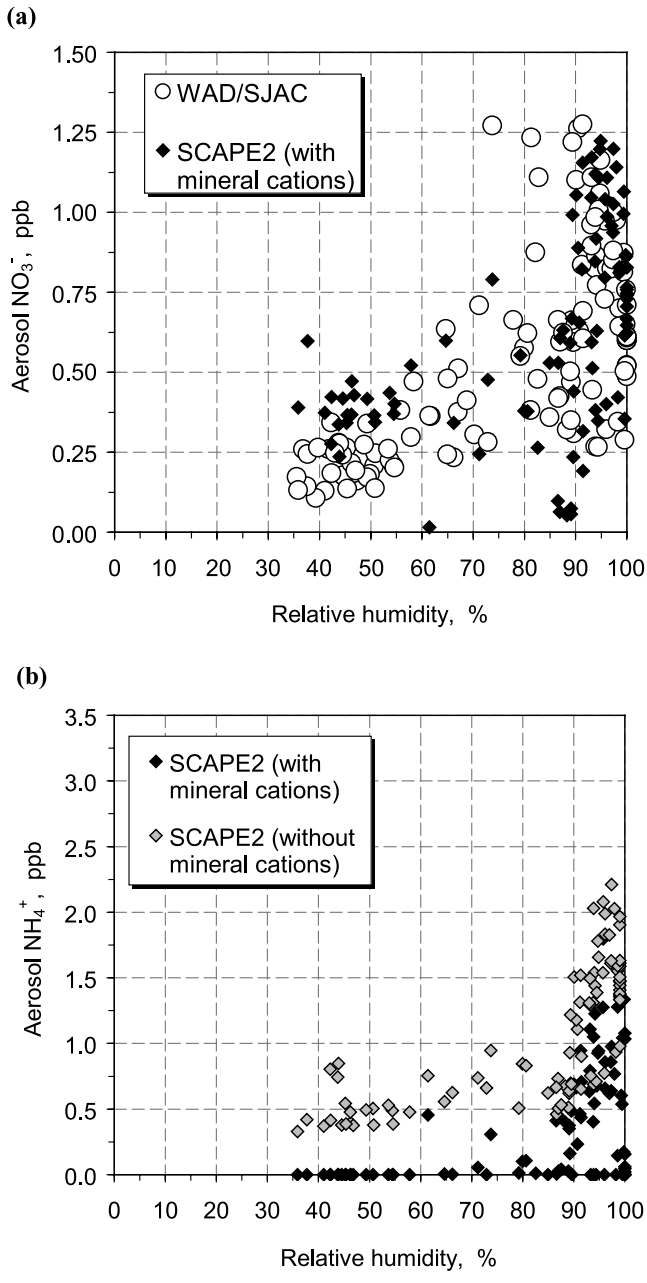

Figure 10. Relative humidity dependence of (a) measured aerosol NO_3^- (PM 2.5) and SCAPE2 predicted aerosol NO_3^- for the K^+-Ca^{2+}-Mg^{2+}-Na^+-HCl/Cl^--NH_3/NH_4^+-HNO_3/NO_3^--H_2SO_4/SO_4^{2-}-H_2O-system and (b) SCAPE2 predicted aerosol NH_4^+ for the system in Figure 10a and SCAPE2 predicted aerosol NH_4^+ for the Na^+-HCl/Cl^--NH_3/NH_4^+-HNO_3/NO_3^--H_2SO_4/SO_4^{2-}-H_2O-system, 17–20 September 2002 dry (biomass burning) season at FNS during LBA-SMOCC 2002.

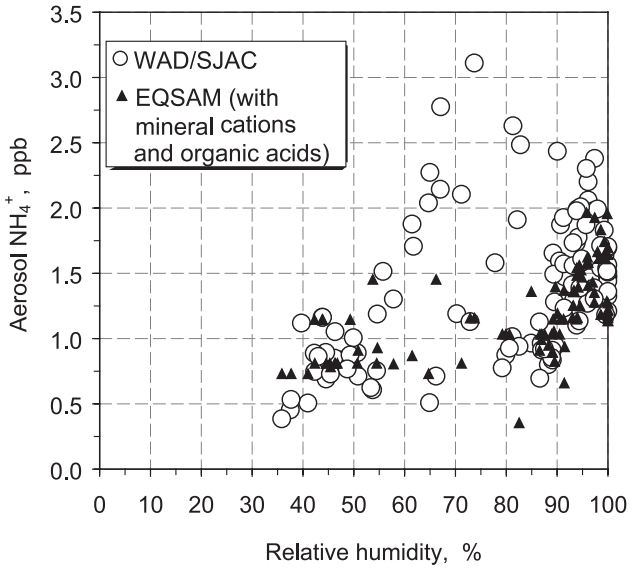

Figure 11. Relative humidity dependence of measured aerosol NH_4^+ (PM 2.5) and EQSAM2 predicted aerosol NH_4^+ for the K^+-Ca^{2+}-Mg^{2+}-Na^+-HCl/Cl^--NH_3/NH_4^+-HNO_3/NO_3^--H_2SO_4/SO_4^{2-}-H_2O-system extended by the sum of equivalent moles of organic acids, 17–20 September 2002 dry (biomass burning) season at FNS during LBA-SMOCC 2002.

[45] However, when the mineral cations are included, the underprediction of fine mode aerosol NH_4^+ by SCAPE2 becomes even larger than before. This is shown in Figure 10b, where aerosol NH_4^+ predicted by SCAPE2 (with and without mineral cations) is plotted versus RH. When mineral cations are included, SCAPE2 does not predict any fine mode aerosol NH_4^+ for RH < 90%, which is in strong contrast to our observations. Obviously, aerosol NH_4^+ is now replaced by other cations (mineral species, especially K^+) which preferentially balance NO_3^-, Cl^- and SO_4^{2-}. According to the model simulations, aerosol NH_4^+ would only be present at RH > 90%, when thermodynamic equilibrium permits the formation of aqueous NH_4NO_3 and NH_4Cl. This implies that at lower RH during daytime, fine mode NO_3^-, Cl^- and SO_4^{2-} are solely balanced by mineral cations (especially K^+), revising the ion balance presented in Figure 6a. These findings are supported by a study by *Li et al.* [2003], who found that smoke particles emitted by biomass fires in Southern Africa were dominated by potassium salts. Primary KCl-containing particles are emitted by biomass fires, and ageing of biomass smoke may lead to displacement of Cl from the aerosol phase [*Li et al.*, 2003, and references therein]. The analogous mechanism is known for sea-salt aerosols [e.g., *Ueda et al.*, 2000]. This might be an explanation for the low fraction of aerosol Cl^- observed at the FNS site (see section 3.4 and Figures 5e and 5f).

4.3.3. K^+-Ca^{2+}-Mg^{2+}-Na^+-HCl/Cl^--NH_3/NH_4^+-HNO_3/NO_3^--H_2SO_4/SO_4^{2-}-H_2O-System Including Lumped LMW Polar Organic Acids

[46] The ionic charge balance for the modeled aerosol systems 1 and 2 is not neutral, presumably due to the role of organic acids. Therefore, we investigated the effect of incorporating equivalent lumped LMW polar organic acids into the simplified modeling framework of EQSAM2. This is done by adding the sum of equivalent moles of organic acids (see Table 2c and Figure 6c) to the gas/liquid/solid aerosol system 2, without explicitly modeling the thermodynamics of organic acids. Thus, semivolatility of these species is not taken into account and their effect on aerosol water uptake is assumed to be the same as for other ammonium salts of the same charge. Figure 11 illustrates measured aerosol NH_4^+ and EQSAM2-predicted aerosol NH_4^+ as a function of RH. Due to the inclusion of organic acids, EQSAM2 predicts fine mode aerosol NH_4^+ also for RH < 90%. Compared to aerosol system 2, where solely mineral cations are included (Figure 10b), the modeled aerosol NH_4^+ agrees much better with observations over the entire RH range. These findings indicate that during daytime (RH < 90%) fine mode aerosol NH_4^+ was apparently balanced by organic anions. However, at 65% < RH < 85% EQSAM2 still predicts significantly lower aerosol NH_4^+ mixing ratios than observed with the WAD/SJAC system. This RH range is coincident with the short-term NH_3 spike and aerosol NH_4^+ peak observed around 0900 LT at the FNS site (see Figures 3a and 3b). Apparently, further organic acids in addition to the species included in our study could be present and neutralize excess NH_3 in the aqueous aerosol phase, forming additional NH_4^+. These results provide strong evidence that the presence of polar organic aerosol compounds at our site played an important role in balancing the inorganic aerosol system.

4.4. Overall EQM Performance

[47] In order to underline our findings obtained with SCAPE2 and EQSAM2, model performances of all four

Table 3a. Normalized Mean Error (NME) and Normalized Mean Bias (NMB) of EQSAM2, ISORROPIA, GEFMN, and SCAPE2 for NH_3, HNO_3, HCl, aerosol NH_4^+, NO_3^-, and Cl^- for the Na^+-HCl/Cl^--NH_3/NH_4^+-HNO_3/NO_3^--H_2SO_4/SO_4^{2-}-H_2O-System[a]

	EQSAM2		ISORROPIA		GEFMN		SCAPE2	
System 1	NME, %	NMB, %	NME, %	NMB, %	NME, %	NMB, %	NME, %	NMB, %
NH_3	*33*	*27*	*32*	*25*	*44*	*39*	*31*	*25*
HNO_3	148	129	132	118	146	145	128	113
HCl	37	15	37	19	38	29	36	18
Aerosol NH_4^+	*42*	*−42*	*40*	*−37*	*55*	*−35*	*39*	*−37*
Aerosol NO_3^-	65	−57	58	−52	67	−66	56	−50
Aerosol Cl^-	76	−45	74	−54	84	−84	73	−51

[a]NME and NMB of the four different models are based on WAD/SJAC measurements from the late dry (biomass burning) season, transition period, and the onset of the wet season at FNS during LBA-SMOCC 2002. $NME = \frac{\sum_{i=1}^{n}|M_i - O_i|}{\sum_{i=1}^{n} O_i} \times 100\%$ $NMB = \frac{\sum_{i=1}^{n}(M_i - O_i)}{\sum_{i=1}^{n} O_i} \times 100\%$ with M_i . . . modeled value, O_i . . . observed value.

Table 3b. Normalized Mean Error (NME) and Normalized Mean Bias (NMB) of EQSAM2, ISORROPIA, GEFMN, and SCAPE2 for NH_3, HNO_3, HCl, Aerosol NH_4^+, NO_3^-, and Cl^- for the K^+-Ca^{2+}-Mg^{2+}-Na^+-HCl/Cl^--NH_3/NH_4^+-HNO_3/NO_3^--H_2SO_4/SO_4^{2-}-H_2O-System[a]

	EQSAM2		ISORROPIA		GEFMN		SCAPE2	
System 2	NME, %	NMB, %	NME, %	NMB, %	NME, %	NMB, %	NME, %	NMB, %
NH_3	*55*	*51*	*52*	*47*	*62*	*57*	*52*	*47*
HNO_3	100	5	85	−19	83	−6	82	−18
HCl	42	6	39	−2	34	3	39	−6
Aerosol NH_4^+	*84*	*−84*	*83*	*−83*	*85*	*−84*	*82*	*−82*
Aerosol NO_3^-	43	−2	37	8	38	2	35	8
Aerosol Cl^-	78	−24	69	−6	70	−24	72	−1

[a]NME and NMB of the four different models are based on WAD/SJAC measurements from the late dry (biomass burning) season, transition period, and the onset of the wet season at FNS during LBA-SMOCC 2002. $NME = \frac{\sum_{i=1}^{n}|M_i - O_i|}{\sum_{i=1}^{n} O_i} \times 100\%$ $NMB = \frac{\sum_{i=1}^{n}(M_i - O_i)}{\sum_{i=1}^{n} O_i} \times 100\%$ with M_i . . . modeled value, O_i . . . observed value.

EQMs (EQSAM2, ISORROPIA, GEFMN and SCAPE2) will be compared and discussed briefly for the gas/liquid/solid aerosol systems 1–3. For this purpose, normalized mean error (NME) and normalized mean bias (NMB) of the four EQMs are calculated based on the WAD/SJAC measurements, including data from the dry season, transition period and the wet season (Tables 3a–3c). When modeling the Na^+-HCl/Cl^--NH_3/NH_4^+-HNO_3/NO_3^--H_2SO_4/SO_4^{2-}-H_2O-system, the NME of EQSAM2, ISORROPIA, GEFMN, and SCAPE2 is highest for HNO_3 and aerosol Cl^- (Table 3a). This is mainly caused by the frequent underprediction of aerosol NO_3^- and Cl^- for RH < 90% and the resulting overprediction of gaseous precursors. Consequently, the NMB is negative for all aerosol species and positive for gaseous species. Tables 3a–3c reveal that all EQM results for the simulation of the gas/liquid/solid aerosol system 1 are comparable, which emphasizes that exclusion of mineral cations and organic acids leads to significant deviations of EQM predictions from observations at FNS. Since inorganic aerosol species are underpredicted to a larger extent by GEFMN compared to the other EQMs in the high RH range (see nighttime periods in Figures 8b, 8d, and 8f), NME and NMB values are somewhat higher for GEFMN. This is due to an underestimation of aerosol water at RHs higher than 94%.

[48] Performances of all EQMs change markedly for the K^+-Ca^{2+}-Mg^{2+}-Na^+-HCl/Cl^--NH_3/NH_4^+-HNO_3/NO_3^--H_2SO_4/SO_4^{2-}-H_2O-system (system 2, Table 3b). NME and NMB for aerosol NO_3^- and HNO_3 decrease significantly. However, as discussed before, the inclusion of mineral cations even increases the charge imbalance, such that NME and NMB for gaseous NH_3 and aerosol NH_4^+ are doubled. The predictions of all four EQMs support our previous findings and it is shown that the approach used in EQSAM2 as well as the inclusion of mineral cations as Na^+ equivalent in ISORROPIA and GEFMN are applicable for our aerosol system. Note that, although values given in Tables 3a and 3b represent model runs for PM 2.5 and TSP samples (which include the coarse aerosol fraction), the same overall findings are observed.

[49] NME and NMB values for EQSAM2 simulations incorporating LMW polar organic acids are presented for PM 2.5 measurements only, since not all organic acids were analyzed for the coarse aerosol fraction (Table 3c). The inclusion of organic acids results in a substantial reduction of NME and NMB for aerosol NH_4^+ and NH_3. When mineral cations and organic acids are incorporated, EQSAM2's model bias (NMB) is below ±25% for all inorganic aerosol species and gases (see Tables 3a–3c), confirming the ion balance presented in Figure 6c.

5. Summary and Conclusion

[50] We have measured gaseous NH_3, HNO_3, HCl, SO_2 and their chemically related aerosol species NH_4^+, NO_3^-, Cl^-, and SO_4^{2-} with high time resolution at a pasture site in the Amazon Basin during the late dry season (biomass burning, 12–30 September 2002), the transition period (01–31 October 2002), and the onset of the wet season (clean conditions, 01–14 November 2002). To our knowledge, these are the first real-time measurements of inorganic aerosol species simultaneously with their gaseous precursors in a tropical environment. To derive information about the relevance of mineral cations (K^+, Ca^{2+}, Mg^{2+}) and low molecular weight (LMW) polar organic acids, real-time data were combined with results obtained from the analysis of aerosols collected on 12-, 24-, and 48-hours integrated filter samples. The sampled aerosol was dominated by organic matter. Mixing ratios of NH_3 were one order of magnitude higher than those of acidic gases. Consequently, aerosol NH_4^+ was the dominating inorganic aerosol constituent.

[51] Our analyses, which included simulations using the four thermodynamic equilibrium models, EQSAM2, ISORROPIA, GEFMN, and SCAPE2, suggest the following: (1) High ambient temperatures prevailing in the Amazon region, and low vapor pressure products of $NH_3 \times HNO_3$ and $NH_3 \times HCl$ did not allow formation of aerosol fine mode ($D_p \leq 2.5$ μm) NH_4NO_3 and NH_4Cl at $RH < 90\%$. (2) Thermodynamic equilibrium permitted the formation of aqueous NH_4NO_3 and NH_4Cl during nighttime only ($RH > 90\%$). (3) Mineral cations (especially K^+) present in Amazonian fine mode aerosols significantly balanced

Table 3c. Normalized Mean Error (NME) and Normalized Mean Bias (NMB) of EQSAM2 for NH_3 and Aerosol NH_4^+ (PM 2.5) for the Systems in Tables 3a and 3b Compared to the System in Table 3b Extended by LMW Polar Organic Acids[a]

EQSAM2	System 1		System 2		System 3	
(PM 2.5 only)	NME, %	NMB, %	NME, %	NMB, %	NME, %	NMB, %
NH_3	*29*	*27*	*54*	*53*	*23*	***15***
Aerosol NH_4^+	*40*	*−38*	*86*	*−86*	*31*	***−15***

[a]NME and NMB are based on WAD/SJAC measurements from the late dry (biomass burning) season, transition period, and the onset of the wet season at FNS during LBA-SMOCC 2002.

aerosol NO_3^- and SO_4^{2-}, particularly during daytime. (4) Chloride was largely driven out of the aerosol phase by reaction of pyrogenic KCl with HNO_3 and H_2SO_4. (5) Due to high ratios of NH_3/SO_2 observed at the pasture site, $(NH_4)_2SO_4$ appeared to be only a minor component of the Amazonian fine mode inorganic aerosol. (6) Gaseous NH_3 was largely neutralized by LMW polar organic acids, forming aerosol NH_4^+.

[52] Finally, we like to state that in tropical regions, modeling multiphase equilibria considering only the Na^+-HCl/Cl^--NH_3/NH_4^+-HNO_3/NO_3^--H_2SO_4/SO_4^{2-}-H_2O-system will lead to substantial discrepancies between simulations and observations. This is mainly caused by (1) high RH and high temperatures, (2) the presence of mineral cations in aerosol fine and coarse modes, (3) a significant amount of polar organic compounds, and (4) high NH_3/SO_2 and high NH_4^+/SO_4^{2-} ratios, which are characteristic for tropical regions like the Amazon Basin. To derive valid information about gas/aerosol partitioning and aerosol ionic balances in these regions, it is necessary to include mineral cations into EQM frameworks. Furthermore, our study emphasizes that an explicit thermodynamic approach to simulate the organic/inorganic gas/liquid/solid aerosol system is required. It still needs to be investigated to what extent the water uptake by WSOC-rich aerosols might influence partitioning of inoranic species between gas and aerosol phase.

[53] **Acknowledgments.** The authors gratefully acknowledge financial support by the European Commission (contract EVK2-CT-2001-00110 SMOCC) and by the Max Planck Society. We are thankful to J. von Jouanne and Alcides Camargo Ribeiro for their initiative and support in setting up the sampling location. We further acknowledge S. Pandis for providing the ISORROPIA and GEFMN model, J. H. Seinfeld for providing the SCAPE2 model, and S. Takahama for assistance with the GEFMN model.

References

Allen, A. G., and A. H. Miguel (1995), Biomass burning in the Amazon—Characterization of the ionic component of aerosols generated from flaming and smoldering rain-forest and savanna, *Environ. Sci. Technol.*, *29*(2), 486–493.

Allen, A. G., R. M. Harrison, and J. W. Erisman (1989), Field-measurements of the dissociation of ammonium-nitrate and ammonium-chloride aerosols, *Atmos. Environ.*, *23*(7), 1591–1599.

Andreae, M. O. (1983), Soot carbon and excess fine potassium—Long-range transport of combustion-derived aerosols, *Science*, *220*(4602), 1148–1151.

Andreae, M. O., and P. J. Crutzen (1997), Atmospheric aerosols: Biogeochemical sources and role in atmospheric chemistry, *Science*, *276*(5315), 1052–1058.

Andreae, M. O., et al. (1996), Methyl halide emissions from savanna fires in southern Africa, *J. Geophys. Res.*, *101*(D19), 23,603–23,613.

Andreae, M. O., et al. (2002), Biogeochemical cycling of carbon, water, energy, trace gases, and aerosols in Amazonia: The LBA-EUSTACH experiments, *J. Geophys. Res.*, *107*(D20), 8066, doi:10.1029/2001JD000524.

Andreae, M. O., D. Rosenfeld, P. Artaxo, A. A. Costa, G. P. Frank, K. M. Longo, and M. A. F. Silva-Dias (2004), Smoking rain clouds over the Amazon, *Science*, *303*(5662), 1337–1342.

Ansari, A. S., and S. N. Pandis (1999a), An analysis of four models predicting the partitioning of semivolatile inorganic aerosol components, *Aerosol Sci. Technol.*, *31*(2–3), 129–153.

Ansari, A. S., and S. N. Pandis (1999b), Prediction of multicomponent inorganic atmospheric aerosol behavior, *Atmos. Environ.*, *33*(5), 745–757.

Ansari, A. S., and S. N. Pandis (2000), The effect of metastable equilibrium states on the partitioning of nitrate between the gas and aerosol phases, *Atmos. Environ.*, *34*(1), 157–168.

Artaxo, P., J. V. Martins, M. A. Yamasoe, A. S. Procopio, T. M. Pauliquevis, M. O. Andreae, P. Guyon, L. V. Gatti, and A. M. C. Leal (2002), Physical and chemical properties of aerosols in the wet and dry seasons in Rondonia, Amazonia, *J. Geophys. Res.*, *107*(D20), 8081, doi:10.1029/2001JD000666.

Bassett, M., and J. H. Seinfeld (1983), Atmospheric equilibrium-model of sulfate and nitrate aerosols, *Atmos. Environ.*, *17*(11), 2237–2252.

Bussink, D. W., L. A. Harper, and W. J. Corre (1996), Ammonia transport in a temperate grassland: 2. Diurnal fluctuations in response to weather and management conditions, *Agron. J.*, *88*(4), 621–626.

Cadle, S. H., R. J. Countess, and N. A. Kelly (1982), Nitric-acid and ammonia in urban and rural locations, *Atmos. Environ.*, *16*(10), 2501–2506.

Calvert, J. G., A. Lazrus, G. L. Kok, B. G. Heikes, J. G. Walega, J. Lind, and C. A. Cantrell (1985), Chemical mechanisms of acid generation in the troposphere, *Nature*, *317*(6032), 27–35.

Clegg, S. L., P. Brimblecombe, Z. Liang, and C. K. Chan (1997), Thermodynamic properties of aqueous aerosols to high supersaturation. 2. A model of the system Na^+-Cl^--NO_3^--SO_4^{2-}-H_2O at 298.15 K, *Aerosol Sci. Technol.*, *27*(3), 345–366.

Clegg, S. L., J. H. Seinfeld, and P. Brimblecombe (2001), Thermodynamic modelling of aqueous aerosols containing electrolytes and dissolved organic compounds, *J. Aerosol Sci.*, *32*(6), 713–738.

Crutzen, P. J., and M. O. Andreae (1990), Biomass burning in the tropics—Impact on atmospheric chemistry and biogeochemical cycles, *Science*, *250*(4988), 1669–1678.

Danalatos, D., and S. Glavas (1999), Gas phase nitric acid, ammonia and related particulate matter at a Mediterranean coastal site, Patras, Greece, *Atmos. Environ.*, *33*(20), 3417–3425.

Erisman, J. W., A. W. M. Vermetten, W. A. H. Asman, A. Waijers-Ijpelaan, and J. Slanina (1988), Vertical-distribution of gases and aerosols—The behavior of ammonia and related components in the lower atmosphere, *Atmos. Environ.*, *22*(6), 1153–1160.

Falkovich, A. H., E. R. Graber, G. Schkolnik, Y. Rudich, W. Maenhaut, and P. Artaxo (2005), Low molecular weight organic acids in aerosol particles from Rondonia, Brazil, during the biomass-burning, transition and wet periods, *Atmos. Chem. Phys.*, *5*, 781–797.

Fisch, G., J. Tota, L. A. T. Machado, M. Dias, R. F. D. Lyra, C. A. Nobre, A. J. Dolman, and J. H. C. Gash (2004), The convective boundary layer over pasture and forest in Amazonia, *Theor. Appl. Climatol.*, *78*(1–3), 47–59.

Fridlind, A. M., and M. Z. Jacobson (2000), A study of gas-aerosol equilibrium and aerosol pH in the remote marine boundary layer during the First Aerosol Characterization Experiment (ACE 1), *J. Geophys. Res.*, *105*(D13), 17,325–17,340.

Graham, B., et al. (2003a), Composition and diurnal variability of the natural Amazonian aerosol, *J. Geophys. Res.*, *108*(D24), 4765, doi:10.1029/2003JD004049.

Graham, B., P. Guyon, P. E. Taylor, P. Artaxo, W. Maenhaut, M. M. Glovsky, R. C. Flagan, and M. O. Andreae (2003b), Organic compounds present in the natural Amazonian aerosol: Characterization by gas chromatography-mass spectrometry, *J. Geophys. Res.*, *108*(D24), 4766, doi:10.1029/2003JD003990.

Gupta, A., R. Kumar, K. M. Kumari, and S. S. Srivastava (2003), Measurement of NO_2, HNO_3, NH_3 and SO_2 and related particulate matter at a rural site in Rampur, India, *Atmos. Environ.*, *37*(34), 4837–4846.

Guyon, P., B. Graham, J. Beck, O. Boucher, E. Gerasopoulos, O. L. Mayol-Bracero, G. C. Roberts, P. Artaxo, and M. O. Andreae (2003), Physical properties and concentration of aerosol particles over the Amazon tropical forest during background and biomass burning conditions, *Atmos. Chem. Phys.*, *3*, 951–967.

Harrison, R. M., and I. M. Msibi (1994), Validation of techniques for fast-response measurement of HNO_3 and NH_3 and determination of the $[NH_3]$ $[HNO_3]$ concentration product, *Atmos. Environ.*, *28*(2), 247–255.

Harrison, R. M., and C. A. Pio (1983), An investigation of the atmospheric HNO_3-NH_3-NH_4NO_3 equilibrium relationship in a cool, humid climate, *Tellus, Ser. B*, *35*(2), 155–159.

Hegg, D. A., L. F. Radke, P. V. Hobbs, and P. J. Riggan (1988), Ammonia emissions from biomass burning, *Geophys. Res. Lett.*, *15*(4), 335–337.

Hesterberg, R., A. Blatter, M. Fahrni, M. Rosset, A. Neftel, W. Eugster, and H. Wanner (1996), Deposition of nitrogen-containing compounds to an extensively managed grassland in central Switzerland, *Environ. Pollut.*, *91*(1), 21–34.

Hildemann, L. M., A. G. Russell, and G. R. Cass (1984), Ammonia and nitric-acid concentrations in equilibrium with atmospheric aerosols—Experiment vs. theory, *Atmos. Environ.*, *18*(9), 1737–1750.

Kerminen, V. M., R. Hillamo, K. Teinila, T. Pakkanen, I. Allegrini, and R. Sparapani (2001), Ion balances of size-resolved tropospheric aerosol samples: Implications for the acidity and atmospheric processing of aerosols, *Atmos. Environ.*, *35*(31), 5255–5265.

Khlystov, A., G. P. Wyers, and J. Slanina (1995), The steam-jet aerosol collector, *Atmos. Environ.*, *29*(17), 2229–2234.

Kim, Y. P., and J. H. Seinfeld (1995), Atmospheric gas-aerosol equilibrium 3. Thermodynamics of crustal elements Ca^{2+}, K^{+}, and Mg^{2+}, *Aerosol Sci. Technol.*, *22*(1), 93–110.

Kim, Y. P., J. H. Seinfeld, and P. Saxena (1993), Atmospheric gas aerosol equilibrium 1. Thermodynamic model, *Aerosol Sci. Technol.*, *19*(2), 157–181.

Kirkman, G. A., A. Gut, C. Ammann, L. V. Gatti, A. M. Cordova, M. A. L. Moura, M. O. Andreae, and F. X. Meixner (2002), Surface exchange of nitric oxide, nitrogen dioxide, and ozone at a cattle pasture in Rondonia, Brazil, *J. Geophys. Res.*, *107*(D20), 8083, doi:10.1029/2001JD000523.

Kuhns, H., et al. (2003), The Treasure Valley secondary aerosol study I: Measurements and equilibrium modeling of inorganic secondary aerosols and precursors for southwestern Idaho, *Atmos. Environ.*, *37*(4), 511–524.

Lee, Y. N., et al. (2003), Airborne measurement of inorganic ionic components of fine aerosol particles using the particle-into-liquid sampler coupled to ion chromatography technique during ACE-Asia and TRACE-P, *J. Geophys. Res.*, *108*(D23), 8646, doi:10.1029/2002JD003265.

Li, J., M. Posfai, P. V. Hobbs, and P. R. Buseck (2003), Individual aerosol particles from biomass burning in southern Africa: 2. Compositions and aging of inorganic particles, *J. Geophys. Res.*, *108*(D13), 8484, doi:10.1029/2002JD002310.

Matsumoto, K., and H. Tanaka (1996), Formation and dissociation of atmospheric particulate nitrate and chloride: An approach based on phase equilibrium, *Atmos. Environ.*, *30*(4), 639–648.

Mayol-Bracero, O. L., P. Guyon, B. Graham, G. Roberts, M. O. Andreae, S. Decesari, M. C. Facchini, S. Fuzzi, and P. Artaxo (2002), Water-soluble organic compounds in biomass burning aerosols over Amazonia: 2. Apportionment of the chemical composition and importance of the polyacidic fraction, *J. Geophys. Res.*, *107*(D20), 8091, doi:10.1029/2001JD000522.

Mehlmann, A., and P. Warneck (1995), Atmospheric gaseous HNO_3 particulate nitrate, and aerosol-size distributions of major ionic species at a rural site in western Germany, *Atmos. Environ.*, *29*(17), 2359–2373.

Meng, Z. Y., and J. H. Seinfeld (1996), Time scales to achieve atmospheric gas-aerosol equilibrium for volatile species, *Atmos. Environ.*, *30*(16), 2889–2900.

Meng, Z. Y., J. H. Seinfeld, P. Saxena, and Y. P. Kim (1995), Atmospheric gas-aerosol equilibrium 4. Thermodynamics of carbonates, *Aerosol Sci. Technol.*, *23*(2), 131–154.

Metzger, S. (2000), Gas/aerosol partitioning: A simplified method for global modeling, Ph.D. thesis, Univ. of Utrecht, Utrecht, Netherlands. (Available at http://www.library.uu.nl/digiarchief/dip/diss/1930853/inhoud.htm)

Metzger, S., F. Dentener, S. Pandis, and J. Lelieveld (2002), Gas/aerosol partitioning: 1. A computationally efficient model, *J. Geophys. Res.*, *107*(D16), 4312, doi:10.1029/2001JD001102.

Moya, M., A. S. Ansari, and S. N. Pandis (2001), Partitioning of nitrate and ammonium between the gas and particulate phases during the 1997 IMADA-AVER study in Mexico City, *Atmos. Environ.*, *35*(10), 1791–1804.

Nenes, A., S. N. Pandis, and C. Pilinis (1998), ISORROPIA: A new thermodynamic equilibrium model for multiphase multicomponent inorganic aerosols, *Aquat. Geochem.*, *4*(1), 123–152.

Nobre, C. A., G. Fisch, H. R. da Rocha, R. F. D. Lyra, E. P. da Rocha, A. C. L. da Costa, and V. N. Ubarana (1996), Observations of the atmospheric boundary layer in Rondônia, in *Amazonian Deforestation and Climate*, edited by J. H. C. Gash, C. A. Nobre, J. M. E. Roberts, and R. L. Victoria, pp. 413–424, John Wiley, Hoboken, N. J.

Pankow, J. F. (2003), Gas/particle partitioning of neutral and ionizing compounds to single and multi-phase aerosol particles. 1. Unified modeling framework, *Atmos. Environ.*, *37*(24), 3323–3333.

Parmar, R. S., G. S. Satsangi, A. Lakhani, S. S. Srivastava, and S. Prakash (2001), Simultaneous measurements of ammonia and nitric acid in ambient air at Agra (27 degrees 10′N and 78 degrees 05′E) (India), *Atmos. Environ.*, *35*(34), 5979–5988.

Pilinis, C., S. N. Pandis, and J. H. Seinfeld (1995), Sensitivity of direct climate forcing by atmospheric aerosols to aerosol-size and composition, *J. Geophys. Res.*, *100*(D9), 18,739–18,754.

Pio, C. A., and R. M. Harrison (1987), Vapor-pressure of ammonium-chloride aerosol—Effect of temperature and humidity, *Atmos. Environ.*, *21*(12), 2711–2715.

Roberts, G. C., P. Artaxo, J. C. Zhou, E. Swietlicki, and M. O. Andreae (2002), Sensitivity of CCN spectra on chemical and physical properties of aerosol: A case study from the Amazon Basin, *J. Geophys. Res.*, *107*(D20), 8070, doi:10.1029/2001JD000583.

Saxena, P., and L. M. Hildemann (1997), Water absorption by organics: Survey of laboratory evidence and evaluation of UNIFAC for estimating water activity, *Environ. Sci. Technol.*, *31*(11), 3318–3324.

Seinfeld, J. H., and S. N. Pandis (1998), *Atmospheric Chemistry and Physics*, pp. 491–541, John Wiley, Hoboken, N. J.

Slanina, J., H. M. ten Brink, R. P. Otjes, A. Even, P. Jongejan, A. Khlystov, A. Waijers-Ijpelaan, and M. Hu (2001), The continuous analysis of nitrate and ammonium in aerosols by the steam jet aerosol collector (SJAC): Extension and validation of the methodology, *Atmos. Environ.*, *35*(13), 2319–2330.

Stelson, A. W., and J. H. Seinfeld (1982a), Relative-humidity and temperature-dependence of the ammonium-nitrate dissociation-constant, *Atmos. Environ.*, *16*(5), 983–992.

Stelson, A. W., and J. H. Seinfeld (1982b), Thermodynamic prediction of the water activity, NH_4NO_3 dissociation-constant, density and refractive-index for the NH_4NO_3- $(NH_4)^2SO_4$-H_2O system at 25-degrees-C, *Atmos. Environ.*, *16*(10), 2507–2514.

Stelson, A. W., S. K. Friedlander, and J. H. Seinfeld (1979), Note on the equilibrium relationship between ammonia and nitric-acid and particulate ammonium-nitrate, *Atmos. Environ.*, *13*(3), 369–371.

Talbot, R. W., M. O. Andreae, T. W. Andreae, and R. C. Harriss (1988), Regional aerosol chemistry of the Amazon Basin during the dry season, *J. Geophys. Res.*, *93*(D2), 1499–1508.

Tanner, R. L. (1980), An ambient experimental-study of phase-equilibrium in the atmospheric system - H^{+}, NH_4^{+}, SO_4^{2-}, NO_3^{-} – NH_3 (G), HNO_3 (G), *Abstr. Pap. Am. Chem. Soc.*, *180*, *187-ENVR*.

Trebs, I., F. X. Meixner, J. Slanina, R. P. Otjes, P. Jongejan, and M. O. Andreae (2004), Real-time measurements of ammonia, acidic trace gases and water-soluble inorganic aerosol species at a rural site in the Amazon Basin, *Atmos. Chem. Phys.*, *4*, 967–987.

Ueda, H., T. Takemoto, Y. P. Kim, and W. M. Sha (2000), Behaviors of volatile inorganic components in urban aerosols, *Atmos. Environ.*, *34*(3), 353–361.

Wexler, A. S., and J. H. Seinfeld (1992), Analysis of aerosol ammonium-nitrate—Departures from equilibrium during SCAQS, *Atmos. Environ., Part A*, *26*(4), 579–591.

Wyers, G. P., R. P. Otjes, and J. Slanina (1993), A continuous-flow denuder for the measurement of ambient concentrations and surface-exchange fluxes of ammonia, *Atmos. Environ., Part A*, *27*(13), 2085–2090.

Yamasoe, M. A., P. Artaxo, A. H. Miguel, and A. G. Allen (2000), Chemical composition of aerosol particles from direct emissions of vegetation fires in the Amazon Basin: Water-soluble species and trace elements, *Atmos. Environ.*, *34*(10), 1641–1653.

Zhang, J., W. L. Chameides, R. Weber, G. Cass, D. Orsini, E. Edgerton, P. Jongejan, and J. Slanina (2003), An evaluation of the thermodynamic equilibrium assumption for fine particulate composition: Nitrate and ammonium during the 1999 Atlanta Supersite Experiment, *J. Geophys. Res.*, *108*(D7), 8414, doi:10.1029/2001JD001592.

M. O. Andreae, G. Helas, A. Hoffer, F. X. Meixner, S. Metzger, and I. Trebs, Biogeochemistry and Air Chemistry Departments, Max Planck Institute for Chemistry, P.O. Box 3060, D-55020 Mainz, Germany. (ivonne@mpch-mainz.mpg.de)

P. Artaxo, Instituto de Física, Universidade de São Paulo, Rua do Matão, Travessa R, 187, CEP 05508-900, São Paulo, SP, Brazil.

R. S. da Silva Jr. and M. A. L. Moura, CCEN-Departamento de Meteorologia, Universidad Federal de Alagoas, Campus A. C. Simões BR 104 - km 14, Tabuleiro do Martins, CEP 57072-970, Maceió, Alagoas, Brazil.

A. H. Falkovich and Y. Rudich, Department of Environmental Sciences, Weizmann Institute, 76100 Rehovot, Israel.

J. Slanina, Department of Environmental Sciences, University of Wageningen, Duivendaal 2, 6701 Wageningen, AP, Netherlands.